OUKA
The University of Osaka
Institutional Knowledge Archive

Title	Crystal structure of human monoamine oxidase A at 2.2Å resolution and a functional role of the transmembrane helix
Author(s)	Son, Seyoung
Citation	大阪大学, 2008, 博士論文
Version Type	VoR
URL	https://hdl.handle.net/11094/1452
rights	
Note	

The University of Osaka Institutional Knowledge Archive : OUKA

https://ir.library.osaka-u.ac.jp/

The University of Osaka

理博 12925

Crystal structure of human monoamine oxidase A at 2.2 Å resolution and a functional role of the transmembrane helix

A Doctoral Thesis
by
Seyoung Son

Submitted to the Graduate School of Science
Osaka University
Japan

05, 2008

Crystal structure of human monoamine oxidase A at 2.2 Å resolution and a functional role of the transmembrane helix

(2.2Å 分解能でのヒト由来モノアミン酸化酵素 A の結晶構造と
その膜貫通ヘリックスの機能的役割)

A Doctoral Thesis
by
Seyoung Son

Submitted to the Graduate School of Science
Osaka University
Japan

05, 2008

Acknowledgements

This work has been carried out under the guidance of Professor Tomitake Tsukihara, Institute of Protein Research, Osaka University. I would like to express my deepest thanks for his guidance and encouragement throughout this work.

I would like to thank deeply Dr. Jichun Ma, NIH Center, USA for his kindly advice and discussion. I specially thank from my heart to Dr. Eiki Yamashita and Dr. Yoshimura Masahito, Institute for Protein Research, Osaka University for his appropriate advice and discussion with their technical advices especially about data collection in SPring-8. I also wish to thank deeply Professor Atsushi Nakagawa, Associate Professor Mamorum Suzuki and Dr. Hideaki Tanaka, Institute for Protein Research, Osaka University for their appropriate advices and discussions. I have been greatly inspired by the members of Tsukihara laboratory at Institute for Protein Research, Osaka University. I express my thanks to all members in Tsukihara laboratory for kind assistance and encouragement. Finally, first of all, I would like to thanks to God, and my parents & my all family for their patience and supports.

(Proverbs 16:9 In his heart a man plans his course, but the LORD determines his steps.)

Seyoung Son

Seyoung Son

,2008

Table of contents

Abbreviations

β-ME	β-MercaptoEthanol
DM	Density Modification
DMDPO	Dimethyldecylphosphine oxide
FAD	Flavin Adenin Dinucleotide
k_{cat}	Turnover number; the maximum number of enzymatic reactions catalyzed per second
k_{cat}/K_m	Catalytic efficiency
K_m	Michaelis-Menten constant
MAO	MonoAmine Oxidase
MAOA	MonoAmine Oxidase subtype A
MAOB	MonoAmine Oxidase subtype B
MR	Molecular Replacement
PC12	*n*-Dodecylphosphocholine (Fos-choline 12)
PEG	Polyethylene glycol
PET	positron emission tomography
Tris	Tris(hydroxymethyl)aminomethane
SIR	Single Isomorphous Refraction
SAS	Single wavelength Anomalous Scattering

Chapter 1. Introduction

1-1. Identification of the enzyme

In 1909, Dale and Dixon reported that tyramine (*p*-hydroxyphenylethyl amine)'s effects on an intravenous injection were similar to those effects produced by adrenaline, producing both motor and inhibitory effects of nerves of the sympathetic system (Dale and Dixon, 1909). Hare successfully identified and extracted tyramine oxidase from rabbit liver in 1928 (Hare, 1928). Adrenaline oxidase enzyme was also discovered in 1936 by Balschko *et al.* (Balschko *et al.*, 1936). The enzymes were termed as monoamine oxidase (MAO) in order to distinguish it from diamine oxidase (histaminase) as well as to describe its substrate specificities in 1938 by Zeller (Zeller, 1938).

1-2. Dispute between "one bi-function enzyme" and "two different enzymes"

Many researchers had studied about substrate specificity and inhibitor sensitivity of MAO. On the based of their researches, Hardegg and Heilbronn (1961) suggested that several forms of MAO exist not only in different species but also in several organs of the same species. This suggestion that MAO may exist not as a single enzyme but as several forms was revealed by one research that MAO can be distinguished to two different forms by using the irreversible MAO inhibitor, clorgyline (Johnston, 1968). Johnston termed these enzymes as type A and type B. In 1991 and 1988, the successful isolation of cDNAs of MAOA and MAOB from human (Grimsby *et al.*, 1991) and rat (Ito *et al.*, 1988) finally proved this notion.

Two subtypes of MAO, MAOA and MAOB, have 70% amino acid sequences identity although each enzyme has unique substrate and inhibitor specificities (Figure 1-1) (Bach *et al.*, 1988). MAOA oxidizes serotonin and noradrenaline, while MAOB does not; MAOA is selectively inhibited by clorgyline, while MAOB is highly inhibited by deprenyl.

1-3. Geographical distribution of the enzyme

Some biochemical studies showed that MAOB activity is more abundant in the outer-membrane than in the inner-membrane of rat liver mitochondria (Schnaitman *et al.*, 1967) and the activities of two enzymes are localized in the mitochondria of the rat brain (Student and Edwards, 1977). In addition, MAOA is mainly located in catecholaminergic neurons and astrocytes in the rat brain (Westlund *et al.*, 1993). Based on these reports, one report showed that mitochondria bound MAOA were localized in the whole regions of noradrenergic and dopaminergic neurons as well as serotonergic neurons (Arai *et al.*, 2002).

In human brain, there are geographical differences in MAO activity. The highest levels of activity are shown in the basal ganglia and hypothalamus, whereas the lower activities are observed in the cerebellum and neocortex (O'Carroll *et al.*, 1983). According to the other positron emission tomography (PET) results, the anatomical distribution of labeled inhibitor was found to parallel the distribution of MAOA and MAOB activities in human brain (Fowler *et al.*, 1987). The group showed that two iso-enzymes were not equally distributed in the human brain by using PET, and also showed that the main form in the basal ganglia was MAOB. In this report, they mentioned the necessity of some caution for generalizing results about the activities of some inhibitors obtained from one species to another one. As

an example, MAOA is only involved in dopamine metabolism in the rat brain, whereas both of MAOA and MAOB enzymes can contribute to dopamine metabolism in the human brain (Youdim *et al.*, 2006).

1-4. Purpose of this research

Both enzymes, MAOA and MAOB, are located in a mitochondrial outer-membrane and possess an FAD, as the co-factor, covalently bound to Cys406/397 (MAOA/MAOB) via 8α-(*S*-cysteinyl)-riboflavin linkage (the blue asterisk in Figure 1-1) (Walker *et al.*, 1974). These enzymes catalyze deamination of biogenic and xenobiotic amines, such as neuroactive serotonin (5-HT), norepinephrine (NE), and dopamine (DA) (Figure 1-2). MAO contains a flavin adenine dinucleotide (FAD) covalently bound to a cysteine residue as mentioned above. MAO plays a decisive role in some psychological disorders and other neurological diseases, including depression and Parkinson's disease. Because inhibition of MAO increases the level of neurotransmitters in the central nervous system, developing for the effective inhibitors represents one of the most important approaches to developing novel drugs to treat such the illnesses.

In addition, the oxidative deamination produces harmful hydrogen peroxide which may further generates free radicals (Youdim and Riederer, 1993). In order to develop more effective and specific inhibitors, it is important to understand inhibition and catalytic mechanisms based on the three-dimensional structures.

Development of selective and reversible MAO inhibitors is important not only from the standpoint of treating symptoms (i.e., by increasing the biological halflife of monoamine neurotransmitters), but also with regard to the neuroprotective effects (i.e., prevention or delay of neurodegeneration itself) (Saura *et al.*, 1996).

Binda *et al.* (2002) first determined the X-ray structures of human MAOB at

3.0 Å, and later improved the resolution to 1.7 Å, including co-crystals with various inhibitors (Binda *et al.*, 2003). On the other hand, the structure of MAOA was determined only at lower resolution: Ma *et al.* determined the structure of rat MAOA at 3.2 Å (Ma *et al.*, 2004b), and De Colibus *et al.* (2005) solved the human MAOA structure at 3.0 Å. Despite the limited resolution, we were still able to use these structures to obtain information that was useful to understand the distinct substrate and inhibitor specificities of MAOA and MAOB (Ma *et al.*, 2004b). Interestingly, the X-ray structure of monoclinic human MAOA at 3.0 Å (De Colibus *et al.*, 2005) differs from those of rat MAOA and human MAOB in the loop conformations of residues 108-118 and 210-216, both important components of the active site. These components affect the substrate/inhibitor specificities of human MAOA, as reported previously (De Colibus *et al.*, 2005, Edmondson *et al.*, 2007). From our earlier result, the backbone structure of rat MAOA, including residues 108-118 and 210-216, is nearly identical to that of human MAOB. Because the amino acid sequences of the two enzymes are 70% identical, we had anticipated this similarity. The sequence identity between human MAOA and rat MAOA is as high as 87% over the whole molecule, and 90% in residues 108-118 and 210-216; therefore, in light of their high sequence identity, the structural differences between the two enzymes in these regions are exceptional. Because these regions take parts in the composition of active center, it is therefore important to understand whether the structural differences between rat and human MAOA in these regions exist, because it is critical to verify cautions in generalization of the results between two different species, or whether they are any artifacts, which is critical for the guidance of drug design.

The functional role of the C-terminal transmembrane helix has also been of biological interest. The significance of the binding of MAO to the mitochondrial outer membrane remains unclear. The X-ray structure of rat MAOA revealed that the C-terminus maintains a transmembrane structure (Ma *et al.*, 2004b), while the

present available structures of both human MAOB and monoclinic human MAOA have resolved only a few residues in this helical region (Binda *et al.*, 2003, De Colibus *et al.*, 2005). One report showed that the C-terminal 29 amino acid residues in MAOB are responsible for targeting and anchoring the protein to the mitochondrial outer membrane (Mitoma and Ito, 1992). A C-terminal truncation leads to a significant decrease in MAOB catalytic activity, but does not produce any significant change in inhibitor specificity (Rebrin *et al.*, 2001). Therefore, C-terminal anchoring for this enzyme must be important for its biological functions. From this research, we report the X-ray structure of human MAOA complexed with a reversible MAOA specific inhibitor, harmine, at 2.2 Å resolution. The high-resolution structure provides greater insight into the enzymatic details of MAOA, especially in terms of substrate/inhibitor binding specificities.

Here, we report the X-ray structure of human MAOA complexed with a reversible MAOA specific inhibitor, harmine, at 2.2 Å resolution. The high-resolution structure provides greater insight into the enzymatic details of MAOA, especially in terms of the structure of the substrate/inhibitor binding specificities. We also show whether the structural differences based on the comparisons between rat and human MAOA exist or not.

In addition, we also show human MAOA structure with the full transmembrane helix. We measured activities of wild-type protein as well as mutants with several mutations at residue G110 in loop 108-118, both in the solubilized and membrane-bound forms, in order to better understand the role of the transmembrane anchor.

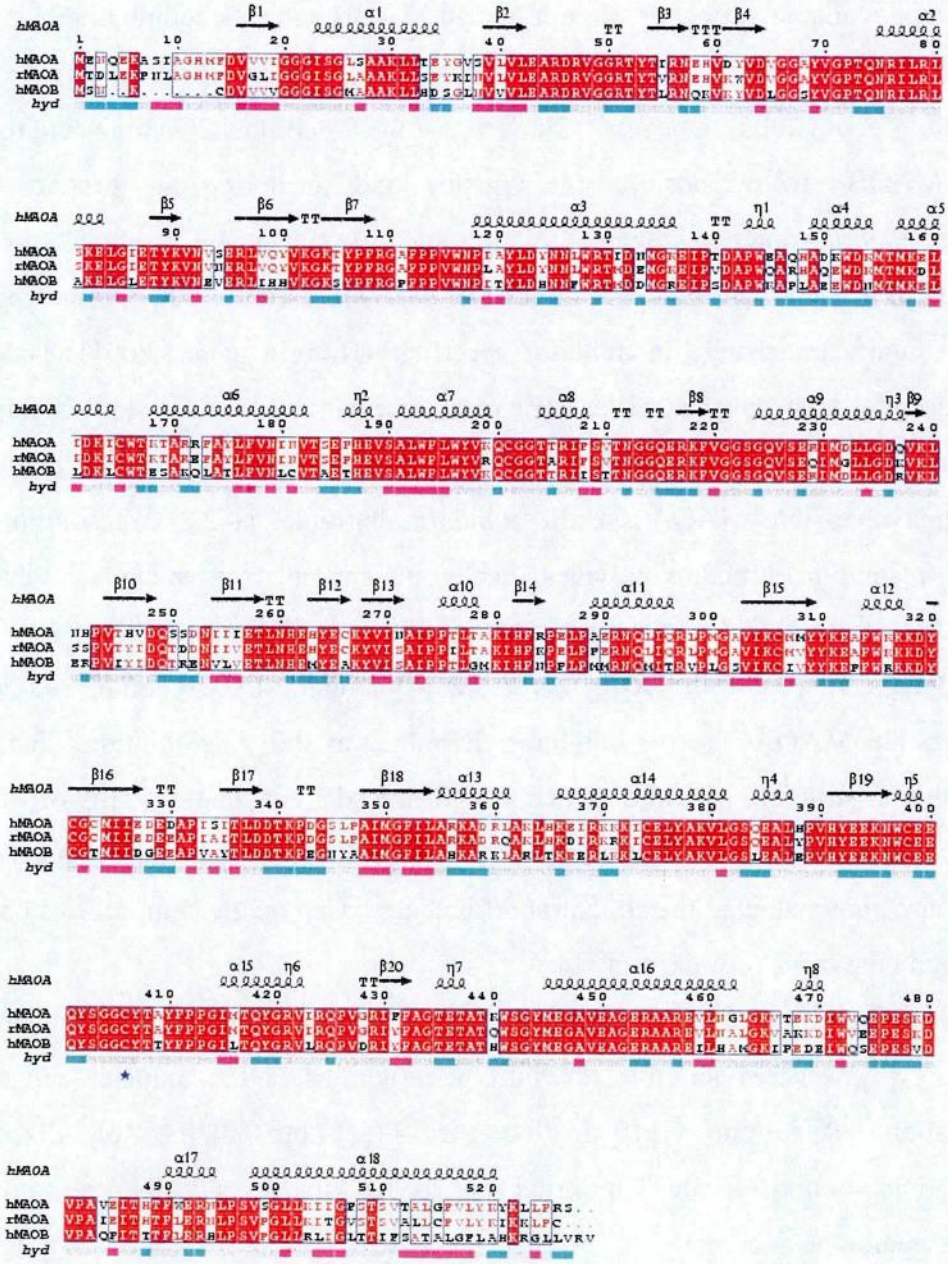

Figure 1-1 Multi-sequence alignments of human and rat MAOA and human MAOB. This alignment was performed by *ClustalW* (Larkin *et al.*, 2007) and was shown by *Espript* program (Gouet *et al.*, 2003). The blue asterisk shows the covalent binding residue Cys406 to FAD.

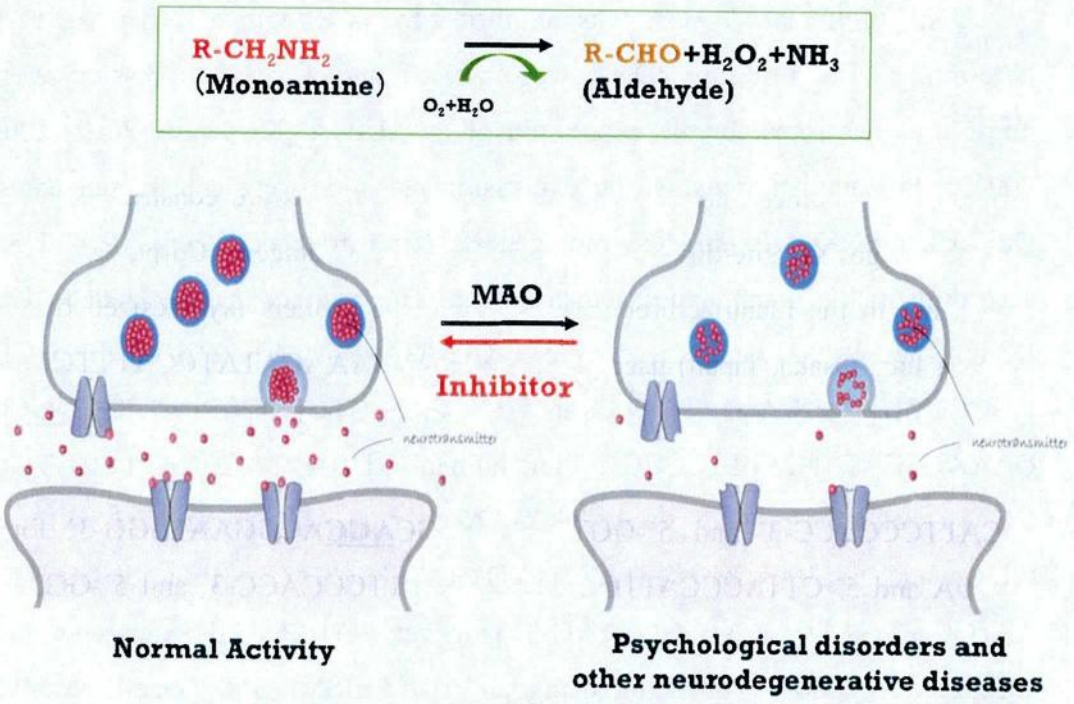

Figure 1-2 Normal and inhibited conditions of MAO enzyme

Chapter 2. Materials and Methods

2-1. Construction of plasmid for expression of wild type and mutants (G110A, G110P) for MAOA

cDNA of human MAOA was amplified by PCR with a 6×His tag at the N-terminus. The resulting cDNA was inserted into a yeast expression vector, YEp51, as described for the expression of rat MAOA (Ma *et al.*, 2002, 2004a, 2004b). For another mutants, the expression plasmids were constructed using a QuickChange XL site-directed mutagenesis Kit (Stratagene Corp., CA, USA), according to the manufacturer's instructions. The primers (synthesized by Gene Design Inc., Osaka, Japan) used were 5'-GGGGAAAACATATCCATTTCGG**GC**
CGCCTTTCCACCAGTATGG-3' and 5'-CCATACTGGTGGAAAGGC**GGC**CC
GAAATGGATATGTTTTCCCC-3' for human G110A, 5'-CCCATTCCGT**GCT**
GCATTCCCACC-3' and 5'-GGTGGGAATGC**AGC**ACGGAATGGG-3' for rat G110A and 5'-CTTACCCATTCCGT**CCT**GCATTCCCACC-3' and 5'-GGTGGG
AATGC**AGG**ACGGAATGGGTAAG-3' for rat G110P. All constructs were confirmed by DNA sequencing using an ABI PRISM 3100 Genetic Analyzer (Applied Biosystems, CA, USA).

2-2. Protein expression and purification

His-tagged wild-type and mutant MAOA proteins were expressed in *Saccharomyces cerevisiae* strain BJ2168 (a prc1-407 prb1122 prp4-3 leu2 trp1 ura3-52) (Wako Pure Chemical Ind., Japan) and purified using a published method (Ma and Ito, 2002).

Briefly, cells transformed with YEp51 vector carrying His-MAOA cDNA were cultured in leucine-free synthesized medium, and expression was induced by galactose for 36 hours.

The detailed protocol of cultivation for human MAOA and the components of the medium are shown to Figure 2-1. After the induction by galactose, the cells were collected by centrifugation at 1,500 g for 10 min and washed with distilled water, and then, treated with yeast lytic enzyme (Zymolyase, Seikagaku Corp. Japan) with gently mixing for 3 hours at 30℃ (50mM Tris-HCl buffer pH7.5, 1M *D*-Glucitol (sorbitol), 10mM $MgCl_2$, 30mM DTT). And then, the cells were collected and treated with yeast lytic enzyme (Zymolyase, Seikagaku Corp., Tokyo, Japan) for 3 hours at 30°C and then disrupted by sonication.

After removing cellular debris by low-speed centrifugation, crude membrane fractions were collected by ultracentrifugation at 40,000 rpm in a Beckman 45-Ti rotor (Beckman Coulter, Inc., CA, USA) for 25 minutes (Figure 2-2). MAOA proteins were solubilized from the crude membrane fraction using *N*-dodecylphosphocholine (Anatrace, Inc., OH, USA) and purified by twice repeats of affinity chromatography on a Ni-column. The purified protein was eluted with buffer containing 500 mM imidazole, and dialyzed against buffer containing 10mM sodium phosphate (pH 7.6), 100 mM sodium chloride, 10% (v/v) glycerol, 5 mM β-mercaptoethanol, and 0.05% (w/v) *N*-dodecylphosphocholine as shown to Figure 2-3.

The final concentration of protein prior to crystallization was 10 mg/ml.

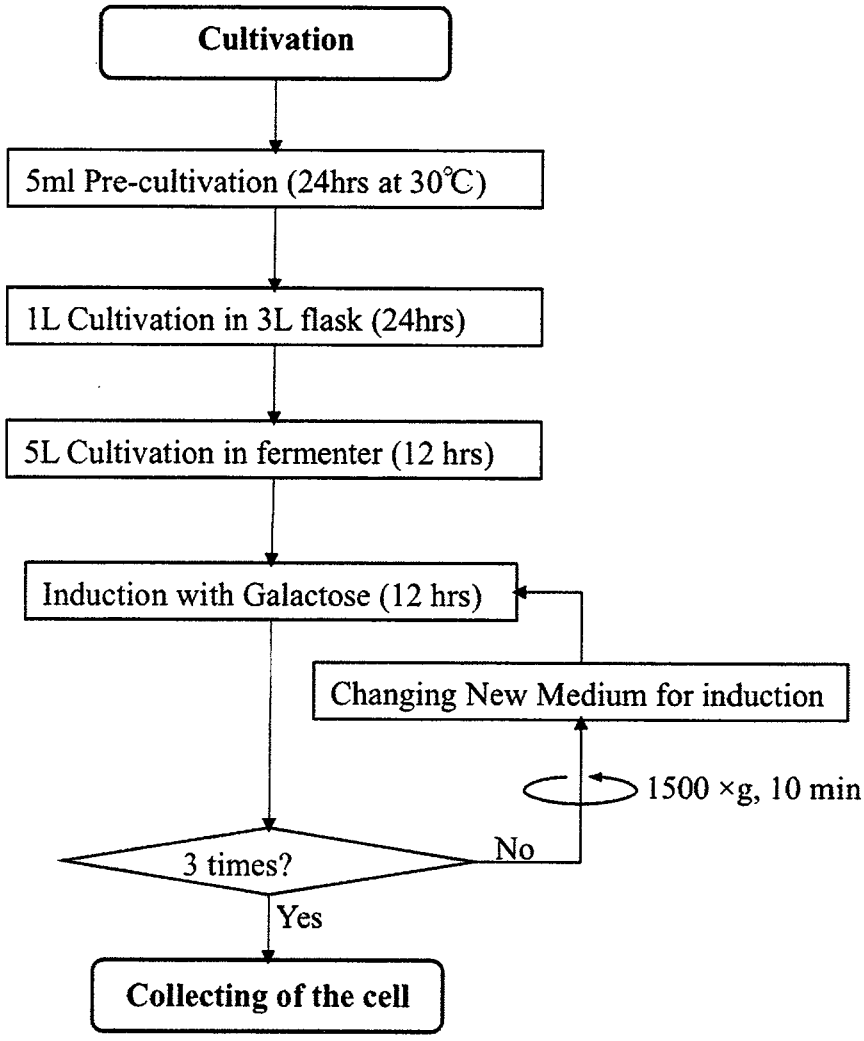

Medium elements in 1 L	
Yeast Nitogen Base	3.0 g
Ammonium Sulfate	5.0 g
Glucose (for cultivation) or Galactose (for induction)	20.0 g
Amine acid mixture (-Leu)	1.6 g

Figure 2-1 Protocol of cultivation for human MAOA and the components of the medium

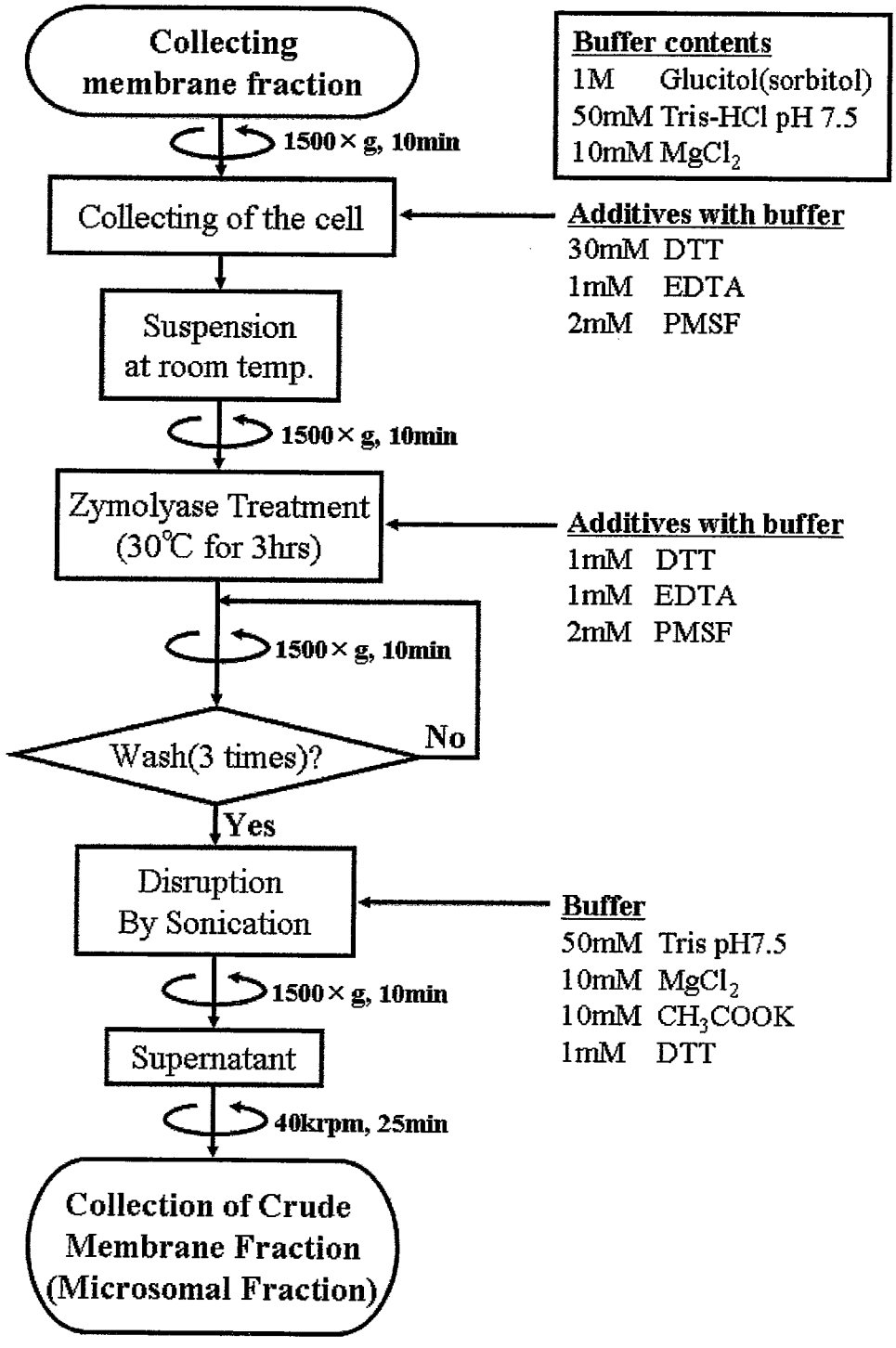

Figure 2-2 Collection protocol of human MAOA for crude membrane fraction

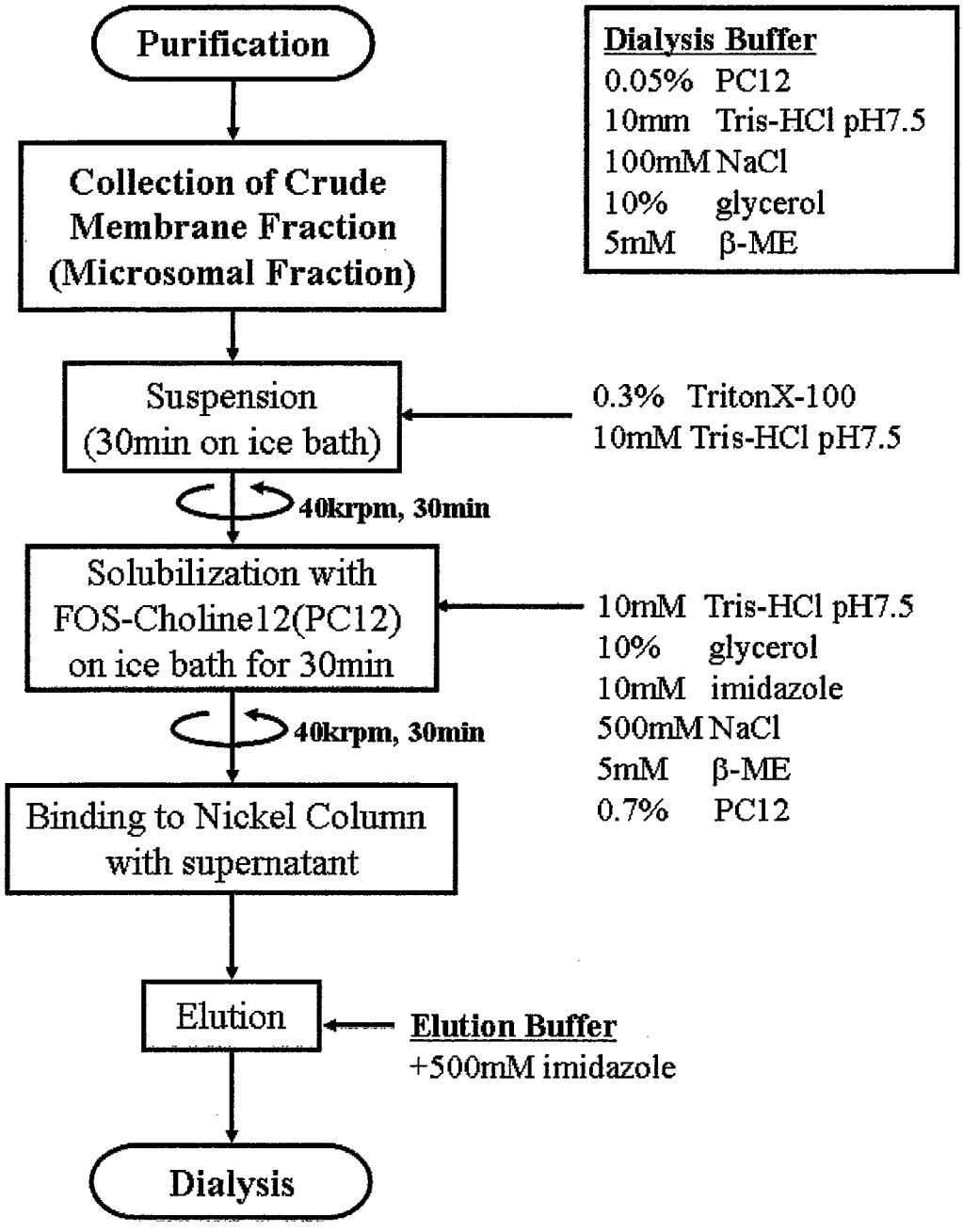

Figure 2-3 Purification protocol of human MAOA from membrane fraction

2-3. Crystallization

2-3-1. Twin crystals

The purified protein after dialysis is used for crystallization.

Initial crystals were obtained by hanging drop vapor diffusion method. Drops were prepared by mixing 2 μl protein solution (10 mg/ml protein solution) and 2 μl reservoir solution (8% PEG4k, 100 mM Phosphate buffer (pH 5.2), 100 mM Sodium acetate, 26% (v/v) Glycerol) and were equilibrated against 0.5 ml reservoir solution at 277 K.

Two detergents were used for this protein, PC12 (dodecylphosphocholine; Fos-coline12) used for isolation, and DMDPO (dimethyldecylphosphine oxide) used for crystallization. Harmine hydrochloride (Wako Pure Chemical Ind., Osaka, Japan), a reversible inhibitor, which promotes the activity of *N,N*-dimethyltrypt -amine in the liver and central nervous system (Callaway *et. al.*, 2005), was co-crystallized with human MAOA.

Harmine hydrochloride was added at a protein : harmine ratio of 1:5. Crystals grew under the same conditions as those for the rat MAOA as low as 3.2 Å resolution. Under the conditions, the crystal could be made with hanging drop vapor diffusion method at 4 °C. The obtained crystals are successfully frozen in the nitrogen gas stream without any additional cryo-protectant at around 100 K. Diffraction of the crystals could be gotten at 2.6 Å resolution (Figure 2-4).

However, all of the crystals were found to be twin. The crystals contained two different patterns in the diffraction. For solving this problem, some kinds of crystallization methods, including seeding method, additive screening and changing crystallization conditions, were tested in this study.

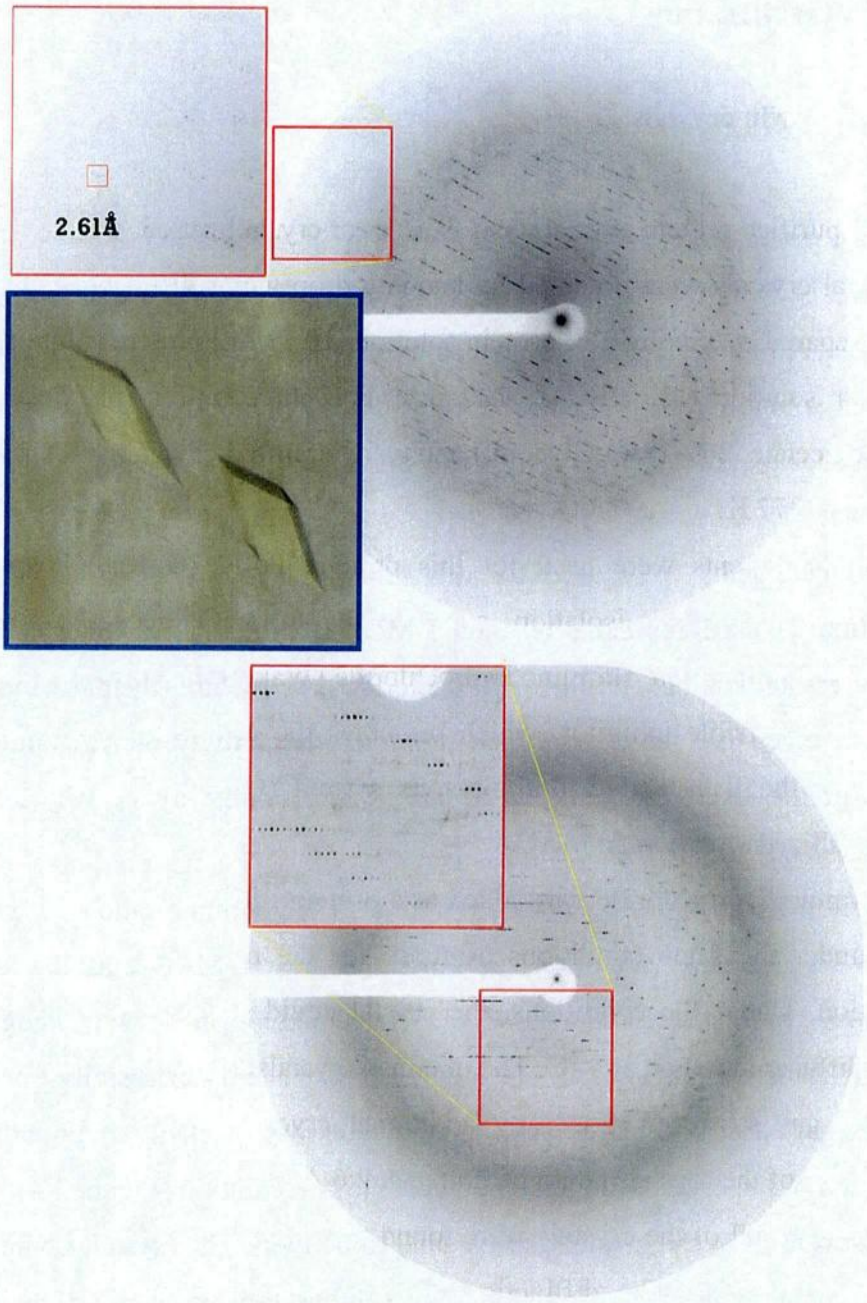

Figure 2-4 Crystal images and the diffraction images of human MAOA under old conditions. The highest diffraction was observed at 2.61Å. Twin diffractions could be shown in below image.

2-3-2. The Solving of twin problem

A. Seeding

Seeding has been critical for obtaining high diffraction-quality crystals for the structure. In this research, we had tried a seeding method to improve the diffraction quality as well as for solving the twin problem.

Streak seeding method, as detailed in Figure 2-5, was used in crystallization step (Stura and Wilson, 1991). Streak seeding methods, technically a micro-seeding method, usually use an animal whisker to touch or stroke over the surface of the protein crystal and then draw through the protein drop (Bergfors, 2003). The principles in the cases of general micro-seeding methods involve the introduction of nucleating agents, like a piece of crystal, into new drops at lower levels of reservoir where controlled. When seeds are introduced at lower levels of reservoir in a crystallization experiment, nucleation may be facilitated and crystal growth initiated (Figure 2-6). Stock solution included seeds was prepared from twin crystals. A few crystals from twin crystals was separately crushed by the micro-needle tool (Hampton Research, CA, USA) after transferring to precipitant drop, including 6% PEG4k, 100 mM phosphate buffer (pH 5.2), 100 mM sodium acetate and 26% (v/v) glycerol, which were used as the seed stocks.

In this method, new crystals which were improved in the diffraction quality but not in solving twin problem could be obtained. In the quality of diffraction, the crystals improved to 2.02-2.37 Å resolution in outer shell, compared to 2.33-2.78 Å resolution in outer shell before seeding (Figure 2-7).

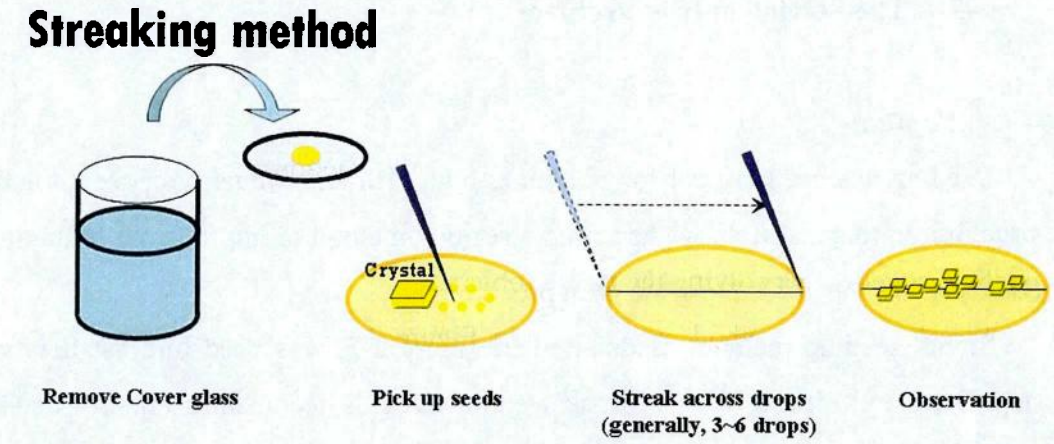

Figure 2-5 The method of streak seeding (Stura and Wilson, 1991)

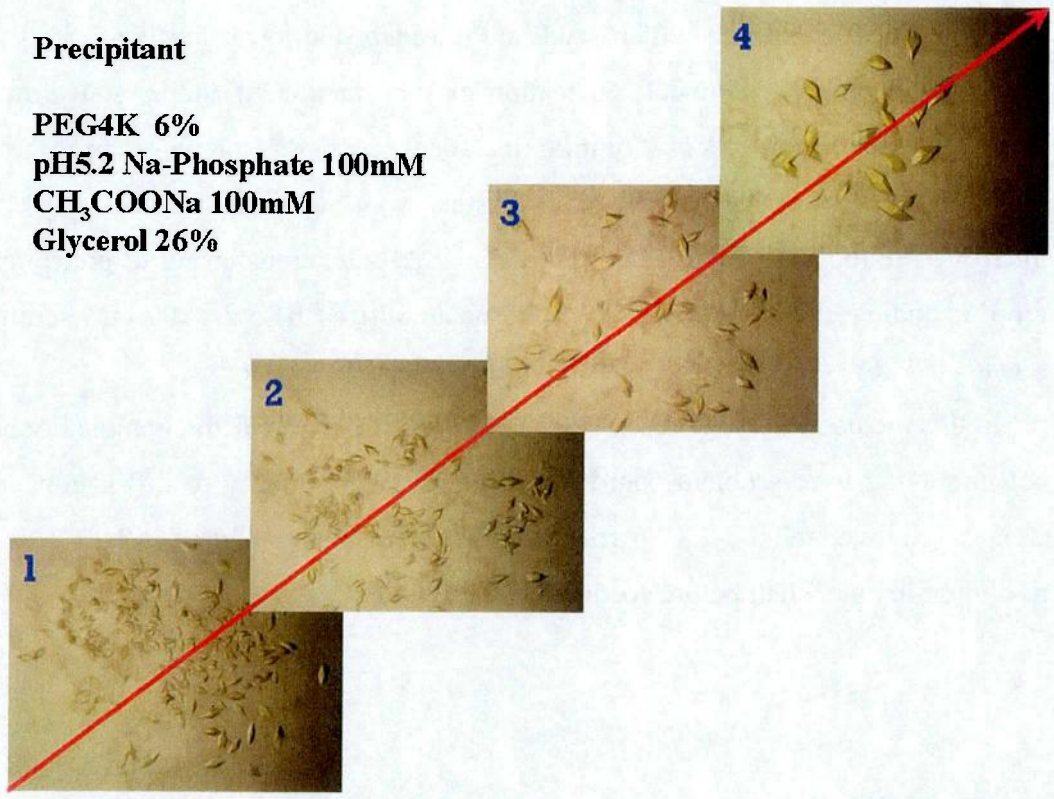

Figure 2-6 Resultant crystals from the streak seeding

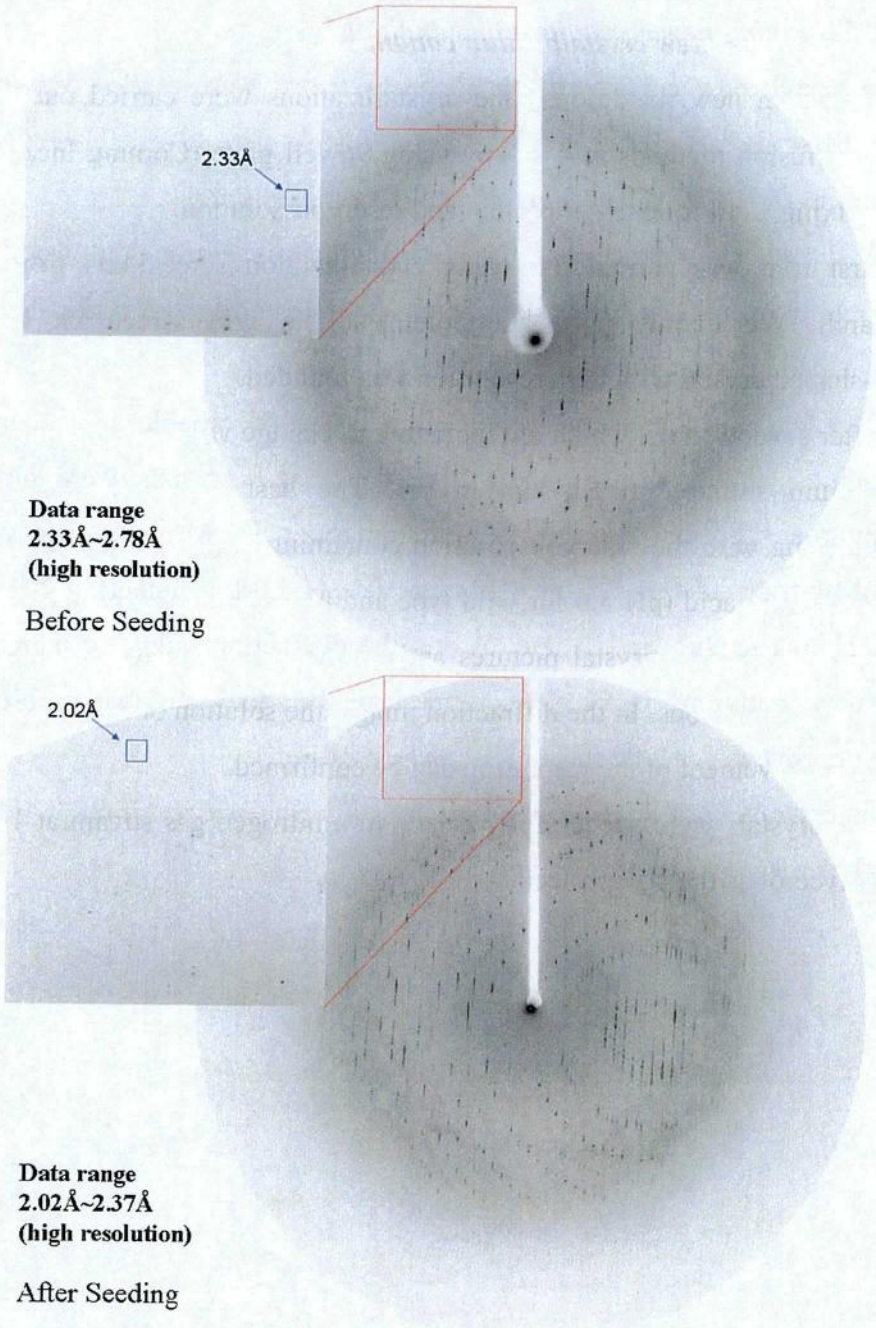

Figure 2-7 Diffraction images before and after seeding. Although the resolution increased to 2.02 Å which was bigger than the resultant before seeding, these crystals were also twins.

B. Searching new crystallization condition

To search new conditions, the crystallizations were carried out sitting-drop vapor diffusion methods at 4 ℃ by using 96well plate (Corning Inc., NY, USA) with mixing 1 μl for each of protein and reservoir solution.

First trial was carried out using crystallization screen kits from Hampton Research. We mainly used ammonium sulfate grid screen kit because the plate-shaped crystal with high resolution was founded.

After several trials, which are including to change variables in concentration of ammonium sulfate, protein and in pH. The best crystals were obtained by equilibrating with the reservoir solution containing 1.6 M ammonium sulfate and 100 mM citric acid (pH 5.6 for wild type and pH 5.0 for mutant) at 277 K. Figure 2-8 is shown to the crystal pictures and the diffraction image of human MAOA under new conditions. In the diffraction image, the solution of twin problem as well as the improvement of the resolution can be confirmed.

The crystals were successfully frozen in a nitrogen gas stream at 100 K using 30% glycerol as the cryoprotectant.

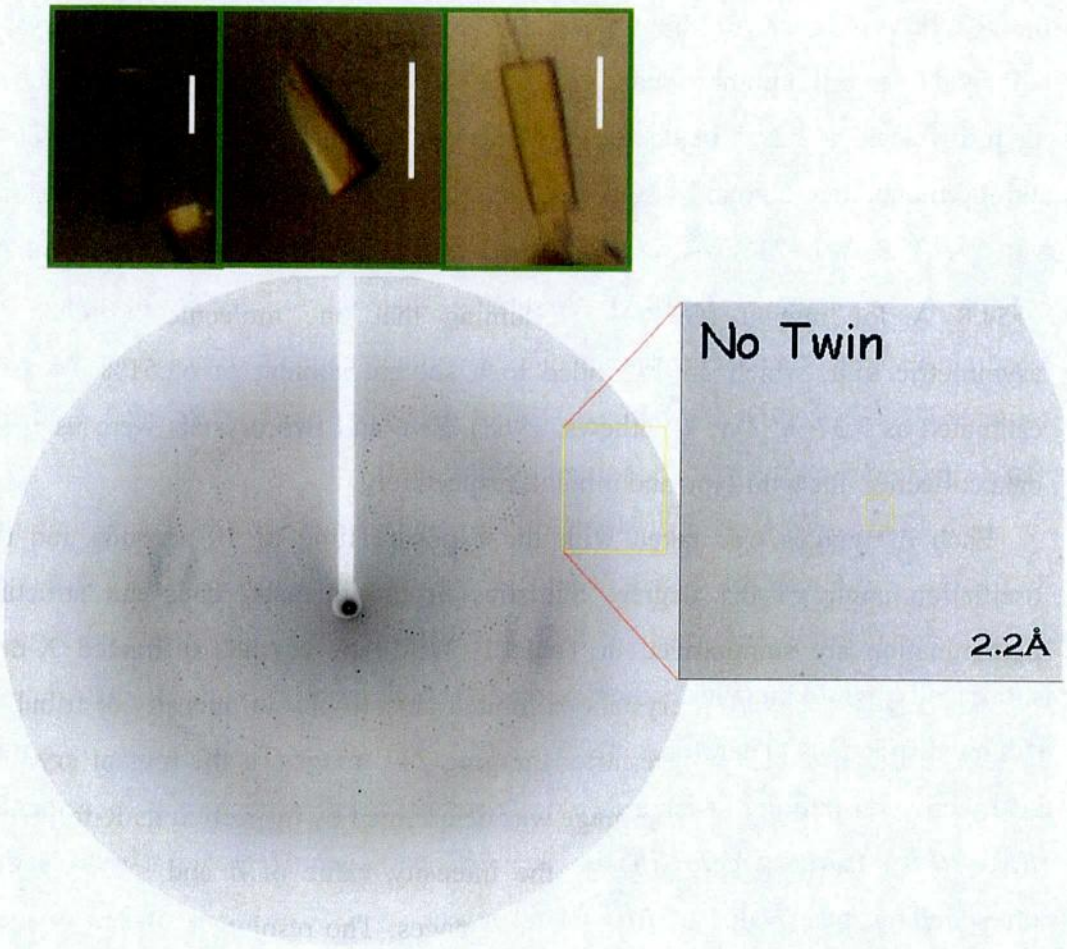

Figure 2-8 The crystal images and the diffraction images of human MAOA under new conditions. From the diffraction image, it can be confirmed the solution of twin problem as well as improvement of the resolution. Scale-bars indicate 50 μm.

2-4. X-ray experiments

The diffraction data were collected at 100 K using an imaging plate detector (DIP6040, Bruker AXS, Tsukuba, Japan) at beamline BL44XU at SPring-8.

Data were indexed and integrated with the MOSFLM program and scaled with the SCALA program in the CCP4suite (Potterton *et al.*, 2003). The crystal belonged to an orthorhombic space group *C*222.

It diffracted at 2.2 Å better than both rat MAOA with $P4_32_12$ (Ma *et al.* 2004) and the monoclinic human MAOA (De Colibus *et al.*, 2005). The cell dimensions were a=135.3 Å, b=218.7 Å, c=54.4 Å for wild-type and a=135.5 Å, b=217.4 Å, c=54.8 Å for mutant (G110A). Assuming that one molecule occupied an asymmetric unit, which corresponded to a solvent content of 63.51%, V_m was estimated as 3.37 $Å^3$ Da^{-1} (Mathews, 1968). Five and two crystals were used for data collection for wild-type and mutant, respectively.

Each of images was taken with the exposure time of 10 seconds and the oscillation angle of 0.5 degree. Statistics of the intensity data and structure determination are summarized in Table 1. Wild-type crystals diffracted X-rays isotropically, while mutant crystals exihibited anisotrophy in intensity distribution of their diffractions. Therefore, after merging 232 images of the mutant crystals, the effective resolution of each image was determined by inspection its R-factor, $\Sigma_h |I(\boldsymbol{h})-\langle I(\boldsymbol{h})\rangle|/\Sigma_h I(\boldsymbol{h})$, where $I(\boldsymbol{h})$ is the intensity value of h and $\langle I(\boldsymbol{h})\rangle$ is the corresponding mean value of $I(\boldsymbol{h})$ for all images. The resolutions of 232 images were different from each other and were in the wide range from 2.17 Å to 3.38 Å.

Table 1 Data collection and refinement statistics

		Wild type	Mutant (G110A)
Beam line		BL44XU (SPring-8, Japan)	
Wavelength (Å)		0.9	
Exposure time (s)		10.0	
Oscillation angle (°)		0.5	
Space group		*C*222	
Cell dimensions	*a* (Å)	135.3	135.5
	b (Å)	218.7	217.4
	c (Å)	54.4	54.8
Resolution range (Å)		60.28-2.20 (2.32-2.20)	49.57-2.16 (2.25-2.16)
Completeness (%)[§]		99.8 (99.7)	71.4(21.5)[a]
Number of unique reflections		41,775 (6.020)	31,614 (1,063)
Redundancy[#]		4.9 (4.9)	2.8 (1.4)
R_{merge}[¶]		0.138 (0.670)	0.079 (0.310)
I/σ[*]		6.7 (1.6)	7.1 (1.5)
Refinement			
R_{cryst}[†]		0.201	0.193
R_{free}[‡]		0.255	0.244
r.m.s.d. [##]	Bonds (Å)	0.023	0.019
	Angle (°)	2.125	1.812
Ramachandran plot			
Allowed region (%)		90.8	90.2
Additionally allowed (%)		8.8	9.4
Generously allowed (%)		0.2	0.2
Disallowed region (%)		0.2	0.2

[a] Completeness (%) was 90.5 (76.8) at 2.55 Å and 94.1 (84.4) at 2.76 Å. #Redundancy was the number of observed reflections for each independent reflection. *$\langle I/\sigma(I)\rangle$ was the average of intensity signal to noise ratio. §Completeness was a percentage of independent reflections observed. ¶R_{merge}, $\Sigma_h\Sigma_i|I(h,i)-\langle I(h)\rangle|/\Sigma_h\Sigma_i I(h,i)$, where $I(h,i)$ was the intensity value of the ith measurement of h and $\langle I(h)\rangle$ was the corresponding mean value of $I(h)$ for all I measurements. The summation was over the reflections with $I/\sigma(I)$ larger than 1.0. †R_{cryst} was a conventional crystallographic R factor, $\Sigma||F_O|-|F_C||/\Sigma|F_O|$, where F_O and F_C were the observed and a calculated structure factor, respectively. ‡R_{free} was a free R factor in the program CNS (Brunger *et al.*, 1998) evaluated for the 5% of reflections that were excluded from the refinement. ##r.m.s.d. represented root mean square deviation.

2-5. Structure determination and refinement

The structure of the wild type protein was determined by the molecular replacement (MR) method using the MOLREP program (Vagin and Teplyakov, 1997). A reference model for molecular replacement was prepared by truncating residues 108-118, 210-216, and 501-527 from rat MAOA (PDB code: 1O5W). The initial phases were calculated at 3.0 Å resolution using the reference model. Since the solvent content of the human MAOA crystal was as high as 63%, phase extension was performed from 3.0 Å to 2.2 Å by the solvent flattening method (Wang, 1985) using the program DM (Cowtan, 1994). The resulting map was referred to as the MR/DM map. The initial model of human MAOA was built on the MR/DM map.

The structure of the mutant was determined by the molecular replacement method using the wild-type structure as a reference model. The MR/DM maps at several resolutions were compared to inspect the effective resolution of the intensity data set. Since the electron density map at 2.17 Å resolution exhibited finer structure than those of the lower resolution, the intensity data up to 2.17 Å were used for the structural refinement of the mutant.

2-5-1. Molecular Replacement (MR) – the principle

Molecular Replacement (MR) is one of the methods to solve the phase problem in X-ray crystal structure determination. A known protein whose structure is similar to the target protein is located in the unit cell of the target protein crystal. Initial phases are estimated for the model crystal consisting of the known protein structures. Fourier synthesis with the initial phases and the observed structure amplitudes produces a crystal structure that is partly the initial model crystal structure and partly the target crystal structure. The structural model of target protein is built in the calculated electron density map and it is used for the structural refinement in the next step. This method is called molecular replacement (MR).

The initial phase determination in MR is required to two steps.

The first step is to determine the orientation of the model structure in the cell of the target molecule by comparing the Patterson function calculated from the known model in a *P*1 cell with that observed structure amplitudes for the crystal of target molecule. This is referred to as the rotation function.

The second step is to determine the position of the correctly oriented model in the cell of the target molecule. This calculation is often referred to as the translation function. (Waller and Dodson, 1993)

<The rotation function>

The rotation function is evaluated with the correlation between Patterson map for the target protein and Patterson map for a crystal consisting of a known molecule. Orientation search (rotation search) is performed by evaluating the correlations for various model crystals each with a different orientation (φ,ψ,χ) from the others.

The rotation function can be expressed as below.

$$C(\varphi,\psi,\chi)=\int_{u,\,v,\,w} P_{target}(u,\,v,\,w)\,P_{model}\{(u,\,v,\,w)\times R(\varphi,\psi,\chi)\}\,du\,dv\,dw$$

C: the value of the rotation function

φ,ψ,χ: each set of rotation angles

$P_{target}(u,\,v,\,w)$: Patterson function of target molecule

$P_{model}(u,\,v,\,w)$: Patterson function of model molecule whose structure is known

$(u,\,v,\,w)$: fractional coordinates

(φ,ψ,χ): rotation matrix

The maximum in this function which exhibit maxima when the two Pattersons have many coincident peaks will tell us the best orientation for placing the phasing model in the unit cell of the desired protein. Near the maximum, the rotation search can be repeated at smaller angular intervals to refine the orientation.

<The translation function>

The translation search is performed in the asymmetric unit cell of native crystal by evaluating the correspondence between the calculated structure amplitudes of the model crystal consisting of a known protein in a given location and the observed structure amplitudes of the native crystal. The standard of the estimation can be expressed as the *R*-factor, which is regarded as a criterion of progress of structure determination. The *R*-factor compares overall coincidence between the amplitudes of two sets of structure factors, as follows.

$$R=\Sigma\,||\boldsymbol{F}_{obs}|-|\boldsymbol{F}_{calc}||\,/\,\Sigma\,|\boldsymbol{F}_{obs}|$$

$|\boldsymbol{F}_{obs}|$: the observed structure-factor amplitude from the native data set

$|\boldsymbol{F}_{calc}|$: the calculated amplitude from the model in its current location

If the observed and calculated intensities coincide to each other in the overall, the numerical differences are small. Because the sum of the differences is smaller than the sum of the intensities themselves, so *R* is smaller than one. All the differences equal zero in perfect agreement, and *R* equals zero.

2-5-2. Density Modification (DM) – the theory

After solution of the phase problem by the isomorphous replacement, the molecular replacement, or the multiple wavelength anomalous dispersion method, the following step is the model building in the electron density map.

If this is successful and the important part in model can be followed in the electron density map, the structural refinement can be started. The poor quality of the electron density map might prevent us from accurate tracing of the model. Wrong structural model may effect in the risk of introducing errors which cannot be easily removed during refinement. When some models were built in poor electron density, the structure may have some undetermined parts or wrong tracing models in important structures. So, in such a case, refinement of the electron density should be preceded through improvement of the protein phase angles.

DM is a general term of the procedure for improving the map with poor density. There are some methods, such as solvent flattening, histogram matching, multi-resolution modification, non-crystallographic symmetry averaging and Sayre's equation technique. (Waller and Dodson, 1993)

Solvent flattening simply involves flattening the density in the solvent region. It is the most common density modification and is powerful to improve phases at fixed resolution, but weak at extending phases to higher resolution.

Histogram matching is a method of image processing, which forces the density to follow the accurate distribution of values. This modification is applied only to the density in the protein region. This method is weaker than solvent flattening for improving phases, but is much more powerful at extending phases to higher resolutions.

Multi-resolution modification is an extension to solvent flattening and histogram matching which allow them to be employed at two resolutions simultaneously. It is fast and fairly powerful across a range of test data.

Non-crystallographic symmetry averaging is one of the most powerful techniques available for improving phases. However it can only be applied when there is non-crystallographic symmetry in the crystal. So, we didn't use this method for these structures because of a monomer in the asymmetric unit, i.e. there is no non-crystallographic symmetry in this crystal for both of them, wild-type and mutant. It requires some additional information, such an averaging mask, describing the parts of the map to be averaged, and averaging operators, describing how the related regions are positioned and oriented. (Rhodes, 2006)

In this research, the solvent flattening and histogram matching are mainly applied for the refinement of electron density. The initial map was composed with a set of reflection data and calculate phases from the model crystal built by the rotation function followed by the translation function. If the phases are poor, the map will be noisy, and it may be difficult to follow the protein main chain. Noise peaks in the solvent region were removed by the solvent flattening. And the modified electron density is back-transformed to give a new phase set. The simplest method for defining a molecular boundary around the protein molecules is by visual inspection of the preliminary electron density map. However, this is rather subjective for a noisy map. An automated method has been proposed by Wang (1985). In the method, the noisy electron density map is smoothed with the next seven steps, as followed Wang (1985).

1. Preparation a data file which contains the phase probability coefficients by the SIR(Single Isomorphous Replacement), the MAD, the SAD or the MR methods.
2. Calculation of a Fourier map with the available phases and observed structure amplitudes.
3. The calculated Fourier map is smoothened by Wang method (1985) to produce a mask which identifies both protein and solvent regions. Each grid point belonging to protein mask is assigned by the electron density with higher value than a threshold level determined from solvent content of the crystal (Wang, 1985).

4. Solvent flattening ; Before this step, a constant density, ρ^C, is added to the entire electron density map such that the average solvent density after adding such a constant will follow the following constraint:

$$(\rho^C+<\rho^{sol}>)/(\rho^C+\rho^{max})=S$$

$<\rho^{sol}>$ and ρ^{max} are meaning the average solvent density and the maximum protein density in the Fourier map, respectively, and S is a constant. Since $F(000)$ is not included in Fourier summation, ρ^C is added to ρ to estimate the electron density at any resolution. S is the averaged electron density of solvent region relative to the maximum electron density of protein region. In theory, if the phases are known the ratio, S can be estimated from knowledge of the protein and solvent composition, the mean temperature factor, and the resolution of the data. Ideally S should be evaluated and compiled from a number of solved structures so that optimal values can be used for the determination of other unknown structures with similar condition. S is empirically given depending on resolution. That of higher resolution map is larger than that of lower resolution. After ρ^C is evaluated from above equation, the removal of the noise in the map, termed solvent flattening, is carried out in the following two conditions: (1) ρ^C is added to the protein of map and any negative density remaining in this region is considered an error and set to zero, and (2) the density in the solvent region is substituted with the new average density, $\rho^C+<\rho^{sol}>$. With the removal of almost the entire noise in the solvent region and part of the noise in the protein region, the map becomes the partial structure of the protein under investigation.

5. Calculation of new structure factors by Fourier transform of the solvent-flattened electron density.

Phase probability, $P_c(\varphi)$, from the solvent flattening is given by the following equation,

$$P_c(\varphi) = N\exp[2|F_o||F_c|/(<|F_o|^2-|F_c|^2>)\cos(\varphi-\varphi_c)],$$

where F_o and F_c are an observed and a calculated structure amplitudes, respectively, and φ_c is a phase angle of the calculated structure factor. N is determined under the normalizing condition, that is, integral $P_c(\varphi)$ is 1.

6. Phase combination Step.

When there are such experimental phase informations as MIR, SIR, MAD and SAD, these experimental phase informations are combined with the phase from the solvent flattening. The phase probability is estimated by joint probability of an experimental phase probability and the phase probability by solvent flattening as follows,

$$P_{comb}(\varphi)=N\, P_o(\varphi)\, P_c(\varphi),$$

Throughout this step, the correct solution in both direct and reciprocal space may be obtained simply through the removal of noise or errors. In other words, this approach may be regarded as a signal (image) enhancement process through error reduction (filtering of errors in direct and reciprocal space).

7. Calculation of the improved map based on $|F_{obs}|$ and α_{com} and a weighting factor of m (Wang, 1985).

The improved electron density map is calculated with coefficients of $m\times|F_{obs}|\times\exp[i\alpha_{comb}]$. Where the weighting factor m and the combined phase α_{comb} are evaluated by the following equations,

$$m\cos(\alpha_{comb}) = \Sigma\, P_{comb}(\varphi)\cos(\varphi) / \Sigma\, P_{comb}(\varphi)$$

and

$$m\sin(\alpha_{comb}) = \Sigma\, P_{comb}(\varphi)\sin(\varphi) / \Sigma\, P_{comb}(\varphi).$$

Procedures from step 2 to step 7 are iterated until the electron density refinement converges well.

2-5-3. Structure refinement

After solving of the phase problem by MR, the REFMAC5 program (Murshudov *et al.*, 1997) was used for structural refinement. The composite-omit-maps which were generated by the CNS (Brünger *et al.*, 1997) were mainly used for remodeling of human MAOA. The Coot program (Emsley and Cowtan, 2004) was used for modeling. Electron density maps were generated by the CNS (Brünger *et al.*, 1997).

Both of proteins, wild-type and mutant (G110A), were one molecule in an asymmetric unit. In order to an inhibitor and additional molecules such as detergents and additives, their geometry libraries were made by using the SKECHER program in the CCP4 suite (Collaborative Computational Project, 1994). During the refinement steps, the all progress was monitored by comparing the measured structure-factor amplitudes $|F_{obs}|$ with $|F_{calc}|$ from the current model. If our structure converged to the correct structure, both of these values used should be converged to each of them, too. Generally, the *residual index*, termed *R*-factor, is well for the confirmation of convergence.

$$R=\Sigma_h \, ||\boldsymbol{F}(\boldsymbol{h})_{obs}|-k|\boldsymbol{F}(\boldsymbol{h})_{calc}|| \, / \, \Sigma_h \, |\boldsymbol{F}(\boldsymbol{h})_{obs}|$$

Sometimes, *R*-factor is calculated at low resolution with a wrong model in a refinement step because of over fitting problem. In order to avoid its problem, *R* free is used during the refinement step. In general, 5~10% reflections are randomly selected for the R_{free} calculation, but are not used during the refinement steps. If the correct model were built, both *R*-factor and R_{free}-factor would exhibit low values. *R*-factor is related to the resolution. Reasonable structure for these models should give an *R* no greater than (resolution)/10. For example, 2.2 Å model should give *R*-factor smaller than 0.22 in the value. For judging the quality and usefulness of

the refined model, the models were checked using the program PROCHECK. The results of the check, Ramachandran plots, are shown in Figure 3-5, 3-6.

The structure of wild-type human MAOA was refined to R = 0.201 and R_{free} = 0.255 at 2.2 Å resolution. The G110A mutant was isomorphous with the wild type, the mutant structural model was prepared by replacing the residue 110 with alanine; this model refined to R= 0.193 and R_{free}= 0.244 at 2.17 Å resolution.

2-6. Determination of the kinetic properties

The activity of monoamine oxidase A was measured spectrophotometrically by monitoring the increase in absorbance at 314 nm upon oxidation of kynuramine and the formation of 4-hydroxyquinoline (Weissbach *et al.*, 1960) in assay buffer (25 mM Tris pH 7.5, 150 mM NaCl). The concentration of kynuramine ranged from 62.5 μM to 5.0 mM. The extinction coefficient of 4-hydroxyquinoline at 314 nm was determined to be 12,300 M^{-1} cm^{-1}. The kinetic constants were calculated according to the method of Ma and Ito (2002). The concentration of purified MAOA was determined by the absorbance of FAD. The oxidized form of FAD has an absorption peak at 456 nm and an extinction coefficient of 11,800 $M^{-1}cm^{-1}$ (Weyler and Salach, 1985). The concentration of MAOA protein in the mitochondrial outer membrane was determined by titration with an irreversible inhibitor, clorgyline. Briefly, each 10 μl of prepared crude membranes from yeast cells expressing MAO as incubated with 0, 10, 20, 30, 40, 50, 60 80, or 100 *p*mol of clorgyline in assay buffer at room temperature for 2 hours. The remaining enzymatic activity was measured using kynuramine as a substrate, as described above. The minimum concentration of clorgyline that completely inhibited MAOA was considered equivalent to the concentration of the enzyme.

Chapter 3. Results and Discussions

3-1. The overall structure of human monoamine oxidase A

Figure 3-1 shows the overall structure of human MAOA. It is nearly identical to that of rat MAOA, which has ~90% identical sequence to human MAOA. The composite-omit-maps and structural features were coincided with substrate/ inhibitor cavity and the entrance, as well as with other regions including single transmembrane helix.

The C-terminal helix was built by iterations of structural refinements and calculations of composite-omit-maps (Figure 3-2). The statistics of the structural determinations of the wild-type and G110A mutant are shown in Table 1. In the single transmembrane helix from residues 498 to 524, residues 498-521 were fitted uniquely on the composite-omit-map as in Figure 3-3, and converged well to a helical conformation after structural refinement. Although the map at the end of C-terminal region was poor in electron density, the residues, 522-524, were able to be successfully built into the model and their structures converged to a non-helical conformation after refinement. The end three residues, 525-527, were not visible.

The side chains of the transmembrane helix were located in the map, although the B-factors were higher than those of the extra-membrane domain. The averaged B-factor of backbone atoms for the C-terminal helix was 64.2 $Å^2$, while that for the extra-membrane domain was 34.3 $Å^2$. In the mutant, G110A, the B-factor was 65.5 $Å^2$ for the C-terminal helix and 33.5 $Å^2$ for the extra-membrane domain.

The peptide bond between the flavin-substituted Cys-406 and Tyr-407 was in the *cis*-conformation, as was that of human MAOB determined at 1.7 Å resolution as shown in Figure 3-4. The corresponding peptide bond of rat MAOA was not assigned as the *cis*-conformation, because the resolution of the electron density map was too low to determine whether the peptide bond was in the *trans*- or

cis-conformation. It must be the same *cis*-conformation as determined in human MAOA and MAOB. Although the Ramachandran plot for Asp61 of the human MAOA was in the disallowed region, the residue fitted well in the composite-omit-map (Figure 3-5, 3-6).

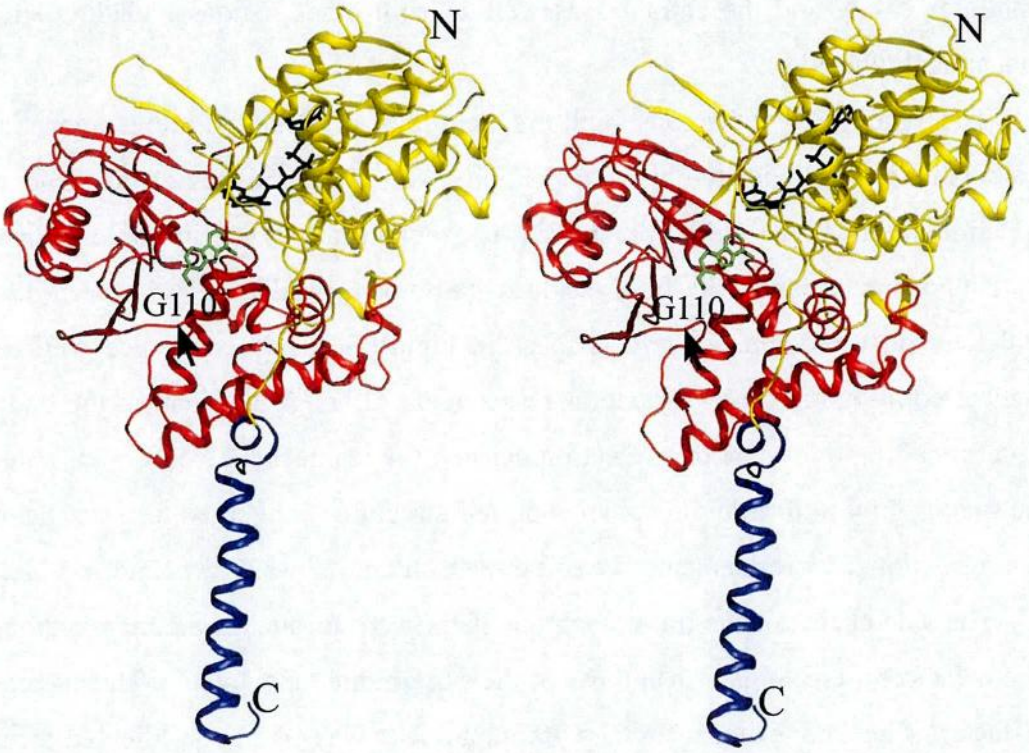

Figure 3-1 Stereoview of the overall structure of human monoamine oxidase A. The picture shows two domains as three parts in different colors. N= N-terminus; C= C-terminus. G110 (black arrow) located on a loop structure near the entrance is the mutation point. The extra-membrane domain consists of the FAD-binding region (yellow) and the substrate/inhibitor binding region (red). The C-terminal single helix transmembrane domain is shown in blue. FAD and harmine molecules are shown in the stick model. Oxygen atoms are shown in red, nitrogen atoms in blue, and other FAD atoms are shown in yellow; Harmine is shown in green. This model was generated by Pymol (DeLano, 2002).

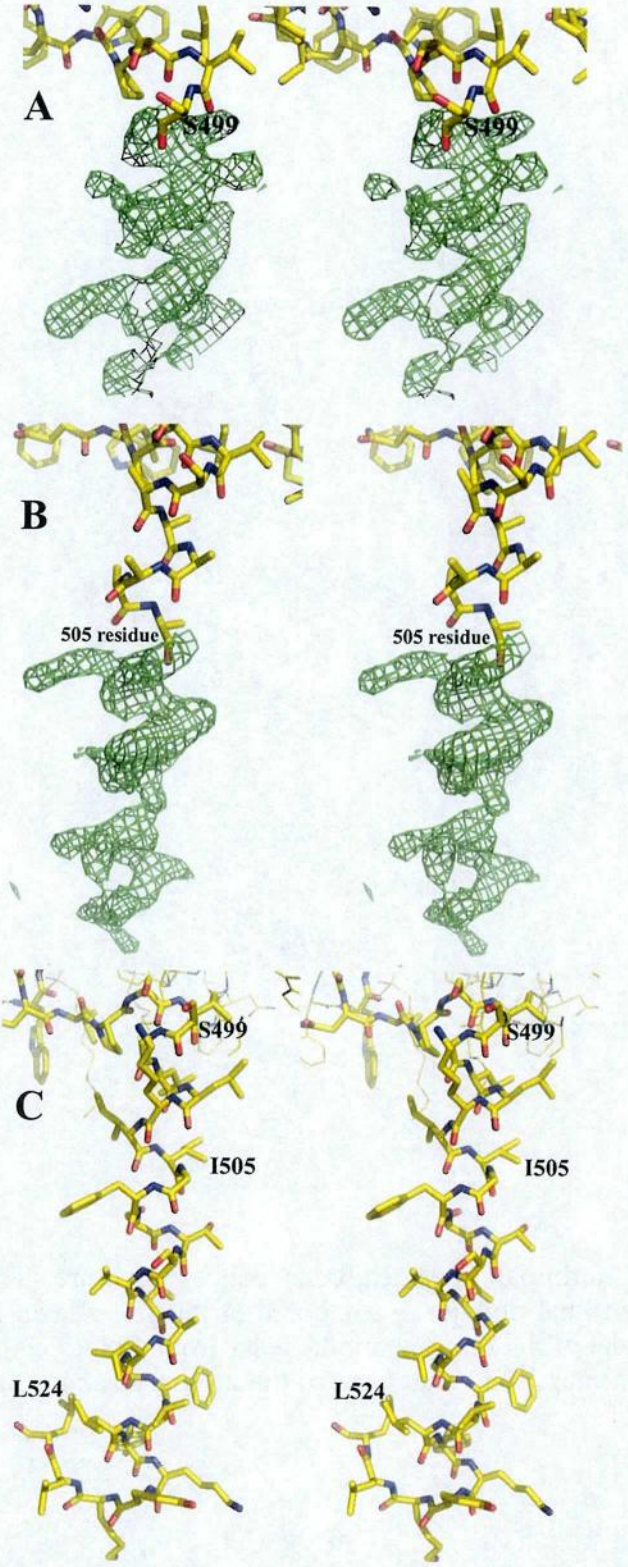

Figure 3-2 Stereoviews of each step for the modeling of the transmembrane helix structure which was built by iteration with several models and Fo-Fc difference Fourier maps. (A) Truncated model from 500- to 524-residue and positively charged Fo-Fc difference Fourier map for the truncated part. (B) Each of five-alanine residues was gradually added to the truncated part until 524-residue in Fo-Fc difference Fourier map. (C) Overall helix-structure which was well changed from the alanine residue to each of specific residue in the map.

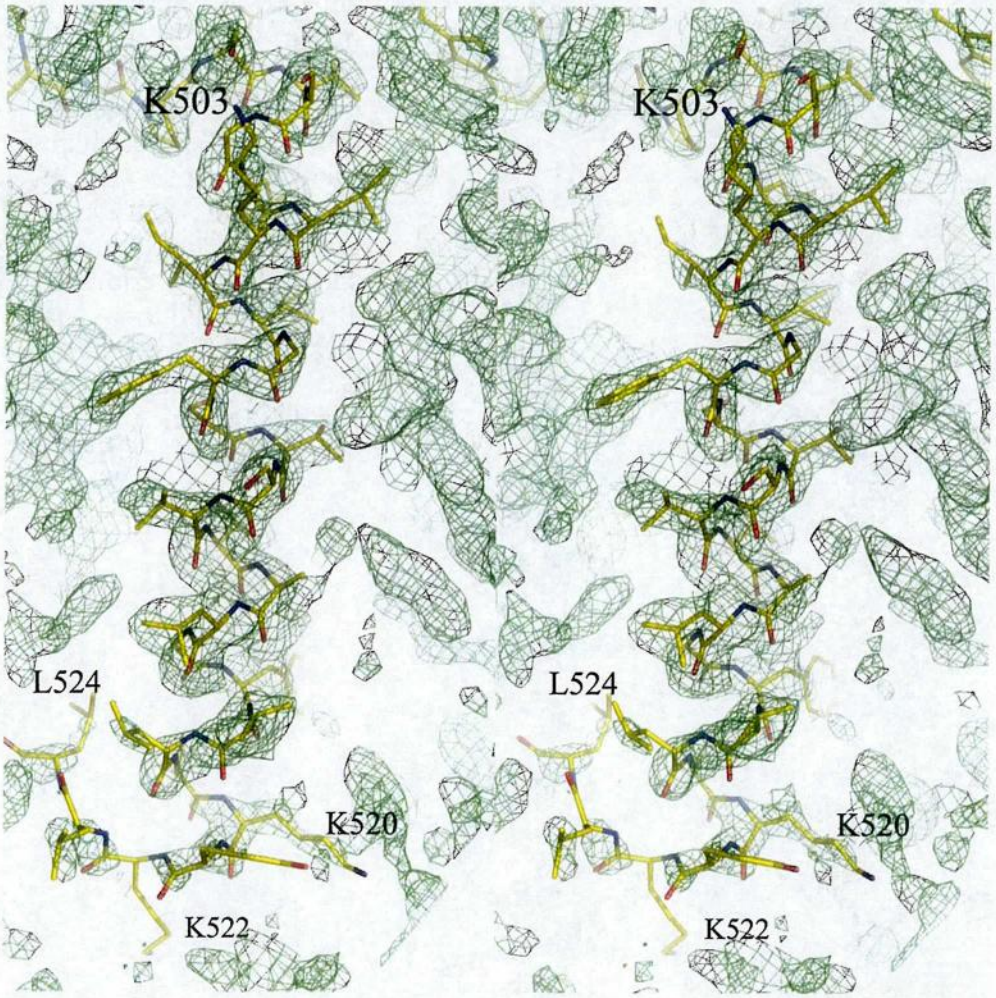

Figure 3-3 Stereoview of the C-terminal transmembrane helical structure. The composite-omit-map for the C-terminal domain is contoured at the 1.0 σ level at 2.2 Å resolution. A structural model of the transmembrane helix from 498 to 524 is superposed on the composite-omit-map. The other parts of the protein structure are not shown for the clarity.

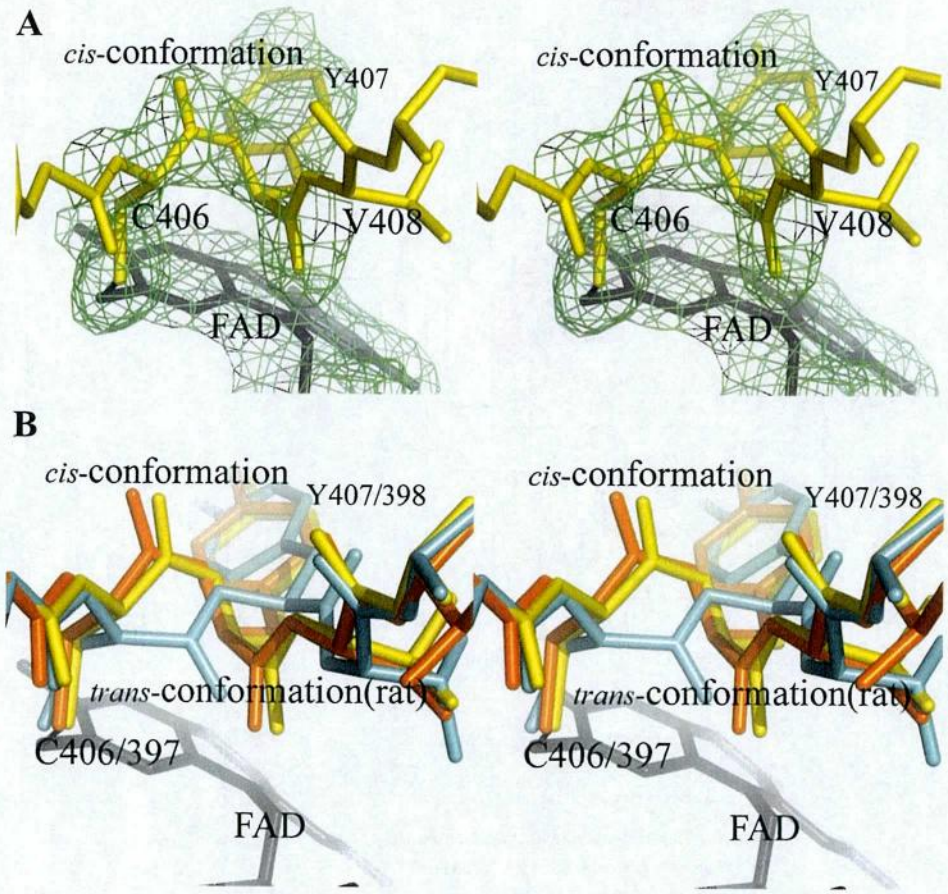

Figure 3-4 Stereoview of (A) *cis*-conformation peptide between C406 and Y407 and its composite-omit-map, and (B) the peptides between human MAOA(yellow), MAOB(orange) and rat MAOA(cyan).

PROCHECK

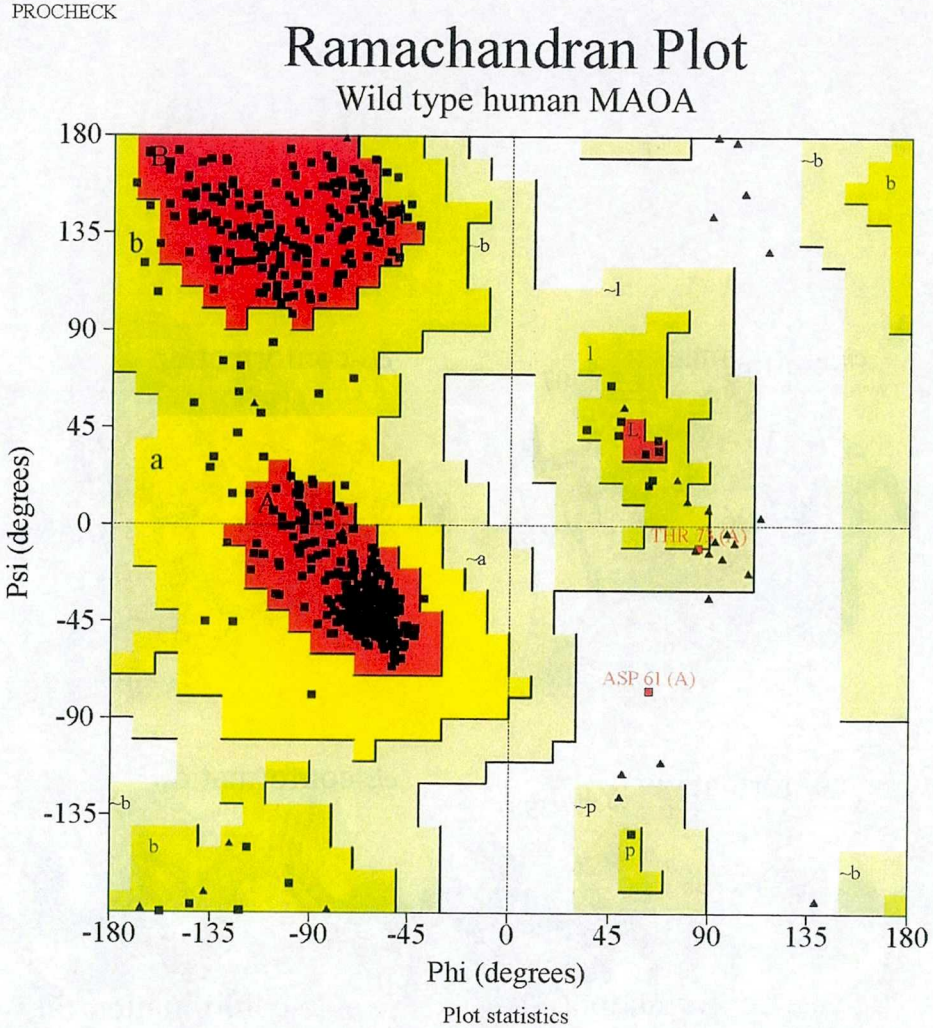

Plot statistics

Residues in most favoured regions [A,B,L]	405	90.8%
Residues in additional allowed regions [a,b,l,p]	39	8.7%
Residues in generously allowed regions [~a,~b,~l,~p]	1	0.2%
Residues in disallowed regions	1	0.2%
Number of non-glycine and non-proline residues	446	100.0%
Number of end-residues (excl. Gly and Pro)	2	
Number of glycine residues (shown as triangles)	41	
Number of proline residues	24	
Total number of residues	513	

Based on an analysis of 118 structures of resolution of at least 2.0 Angstroms and R-factor no greater than 20%, a good quality model would be expected to have over 90% in the most favoured regions.

Figure 3-5 Ramachandran plot for wild type of human MAOA. Asp61 is located in disallowed region.

PROCHECK

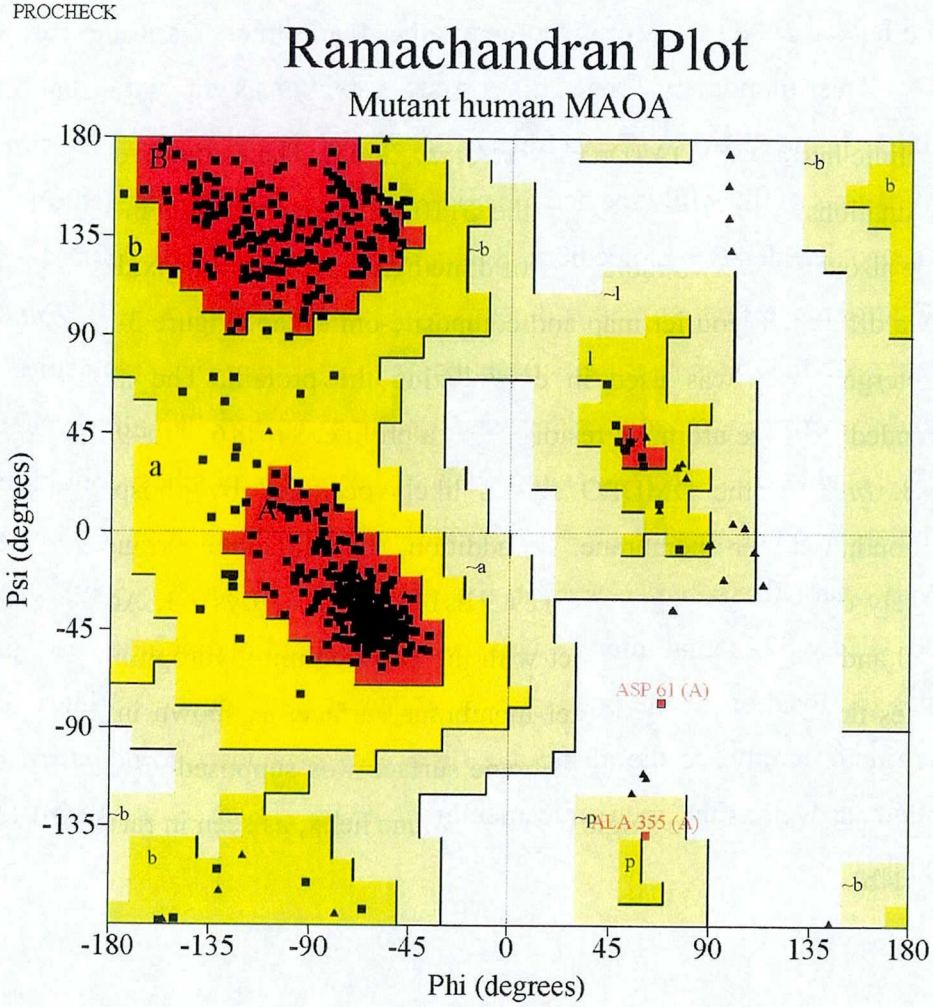

Plot statistics

Residues in most favoured regions [A,B,L]	403	90.2%
Residues in additional allowed regions [a,b,l,p]	42	9.4%
Residues in generously allowed regions [~a,~b,~l,~p]	1	0.2%
Residues in disallowed regions	1	0.2%
Number of non-glycine and non-proline residues	447	100.0%
Number of end-residues (excl. Gly and Pro)	205	
Number of glycine residues (shown as triangles)	40	
Number of proline residues	24	
Total number of residues	716	

Based on an analysis of 118 structures of resolution of at least 2.0 Angstroms and R-factor no greater than 20%, a good quality model would be expected to have over 90% in the most favoured regions.

Figure 3-6 Ramachandran plot for mutant of human MAOA. Asp61 is located in disallowed region.

The human MAOAs were monomers rather than dimers, as in the case of rat MAOA. This monomeric state in crystals was consistent with that of the monoclinic human MAOA (De Colibus *et al.*, 2005). The statistics of the structural determinations of the wild-type and the G110A mutant are shown in Table 1.

We also detected two molecules of dimethyldecylphosphine oxide (DMDPO) in a Fo-Fc difference Fourier map and composite-omit-map (Figure 3-7). DMDPO is the detergent that was used in crystallizing the protein. The molecules were surrounded by three aromatic residues and a proline: Trp116, Trp491, Tyr121, and Pro118. *In vivo*, the DMDPO site is likely occupied by phospholipid in the mitochondrial outer membrane. In addition, the horizontal arrangement of the positively charged residues—Arg129, His148, Lys151, Lys163, Arg493, Lys503, Lys520 and Lys522—that interact with the phospholipid hydrophilic head groups, indicates the location of the outer-membrane surface, as shown in Figure 3-8. A one-turn helix parallel to the membrane surface was supposed to be buried in the membrane, as well as the single transmembrane helix, as seen in rat MAOA (Ma *et al.*, 2004b).

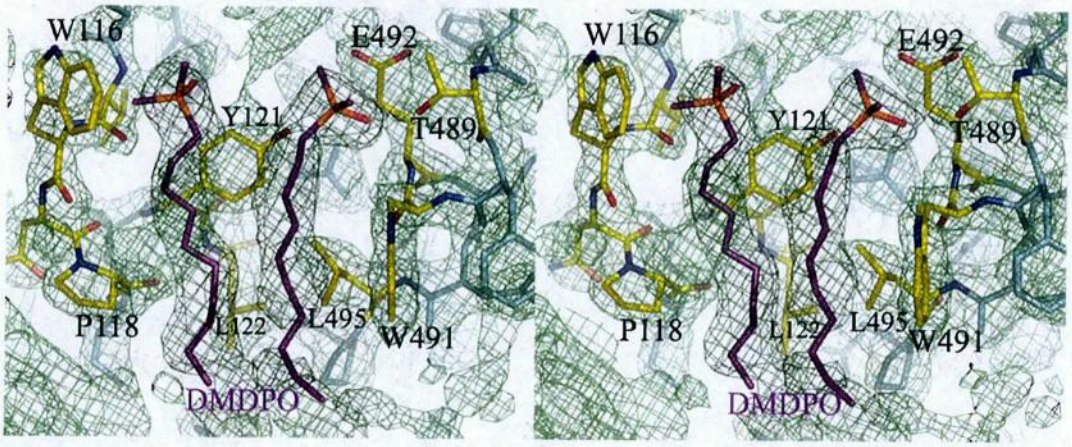

Figure 3-7 The detergent molecules bound at the one-turn helix next to the transmembrane helix. The composite-omit-map (1.0 σ level) was generated by CNSsolve (Brünger *et al.*, 1998). The pocket is surrounded by hydrophobic amino acid residues: W116, P118, Y121, L122, and W491. These models were generated by Pymol (DeLano, 2002).

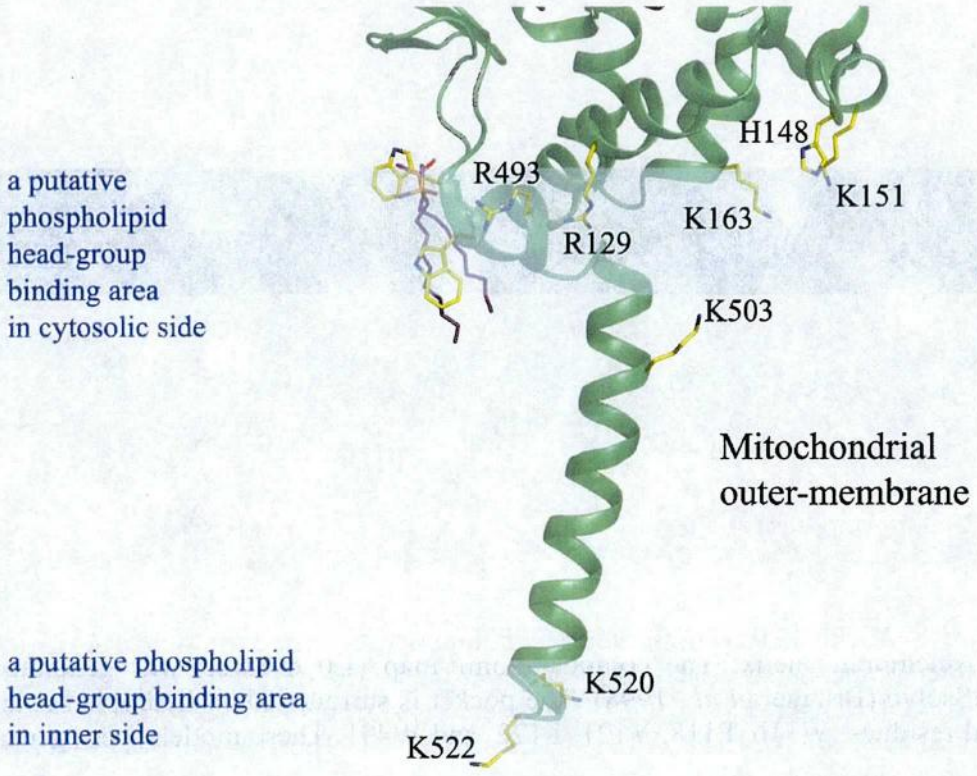

Figure 3-8 Binding model of MAOA into the mitochondrial outer membrane. The positively charged residues Arg129, His148, Lys151, Lys163, Arg493, Lys503, Lys520 and Lys522 are shown. These residues are presumed to interact with the phospholipid hydrophilic head group at membrane surface shown as blue semitransparent areas. The upper area represents the cytosolic side.

3-2. The Structure of the entrance and substrate/inhibitor cavity

The MR/DM and composite-omit-maps and structural features, including B-factors, were coincided with the residues 108-118 and 210-216, which were composed of the entrance and active center cavity, respectively, as well as with other regions. Residues 108-118 and 210-216 of the wild-type human MAOA were clearly assigned in the MR/DM map. The MR/DM and composite-omit-maps and structural features, including B-factors, were reasonable for residues 108-118 and 210-216, as well as for other regions. Residues 108-118 and 210-216 of human MAOA superposed well with the homologous regions of rat MAOA (Ma *et al.*, 2004b), as well as with the corresponding regions of human MAOB (Binda *et al.*, 2003), but differently from those of the earlier reported monoclinic human MAOA (De Colibus *et al.*, 2005). Especially, 210-216 residues are important components for the formation of active center cavity in all kinds of MAO. To double-check the validity of the structure at these regions, we used the monoclinic human MAOA as a search model for the molecular replacement. The resultant maps at the two loop regions did not fit those of the monoclinic human MAOA, but fit our new structure well. A Fo-Fc difference Fourier map had no significant residual density at the residues 108-118 and 210-216 of our structure. These results further confirmed our structure.

Harmine, a reversible inhibitor, is located in the active center cavity of the enzyme. Its chemical structure was shown in Figure 3-9. It interacts with Tyr69, Asn181, Phe208, Val210, Gln215, Cys323, Ile325, Ile335, Leu337, Phe352, Tyr407, Tyr444, and FAD (Figure 3-10). Especially, the amide group of the Gln215 side chain interacts tightly with harmine by a $\pi\square\pi$ interaction with an inter-plane distance of 3.4 Å. Seven water molecules occupy the space between the inhibitor and these groups. The inhibitor and the FAD are bridged through two water molecules by hydrogen bonds. FAD tightly interacts to MAOA protein

through several residues, Ser24, Arg45, Arg51, Tyr69, Val244, Thr435 and Met445 with hydrogen bond, and Ile19, Gly20, Glu43, Ala44, Gly50, Gly66, Gly67, Ile273, Leu277, Val303, Trp397, Tyr407 and Tyr444 with hydrophobic interaction, in human MAOA. In addition, FAD interacts with eight water molecules by hydrogen bond. Some residues, Gly22, Ile23, Gly25, Glu43, Arg45, Arg47, Gly49, Gly50, Gln74, Gln215, Ala272, Tyr402, Ser403, Gln436, and Gln446, are connecting to FAD with hydrogen bond throughout water molecules. Figure 3-11 shows the interactions between FAD and human MAOA in detail.

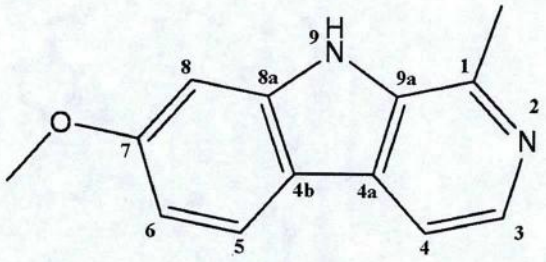

Figure 3-9 The structure of specific reversible inhibitor, harmine.

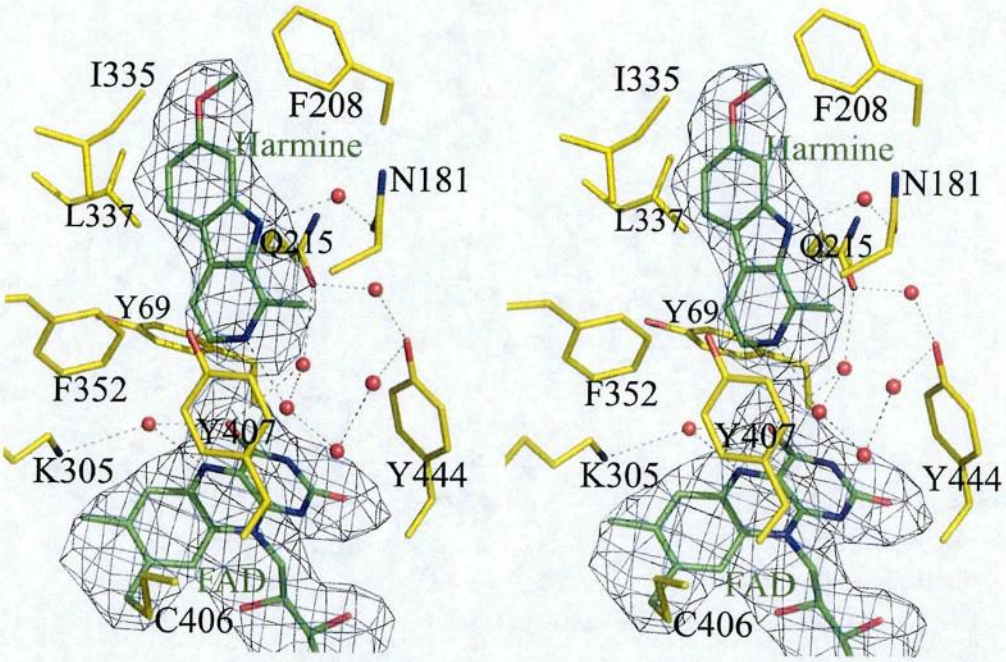

Figure 3-10 Stereoview of the substrate/inhibitor binding site. The Fo-Fc difference Fourier map contoured at 2.0σ was generated at 2.2 Å resolution for the inhibitor (harmine) and FAD. Amino acid residues are shown in yellow, and FAD and harmine are shown in green. Dotted lines indicate hydrogen bonds.

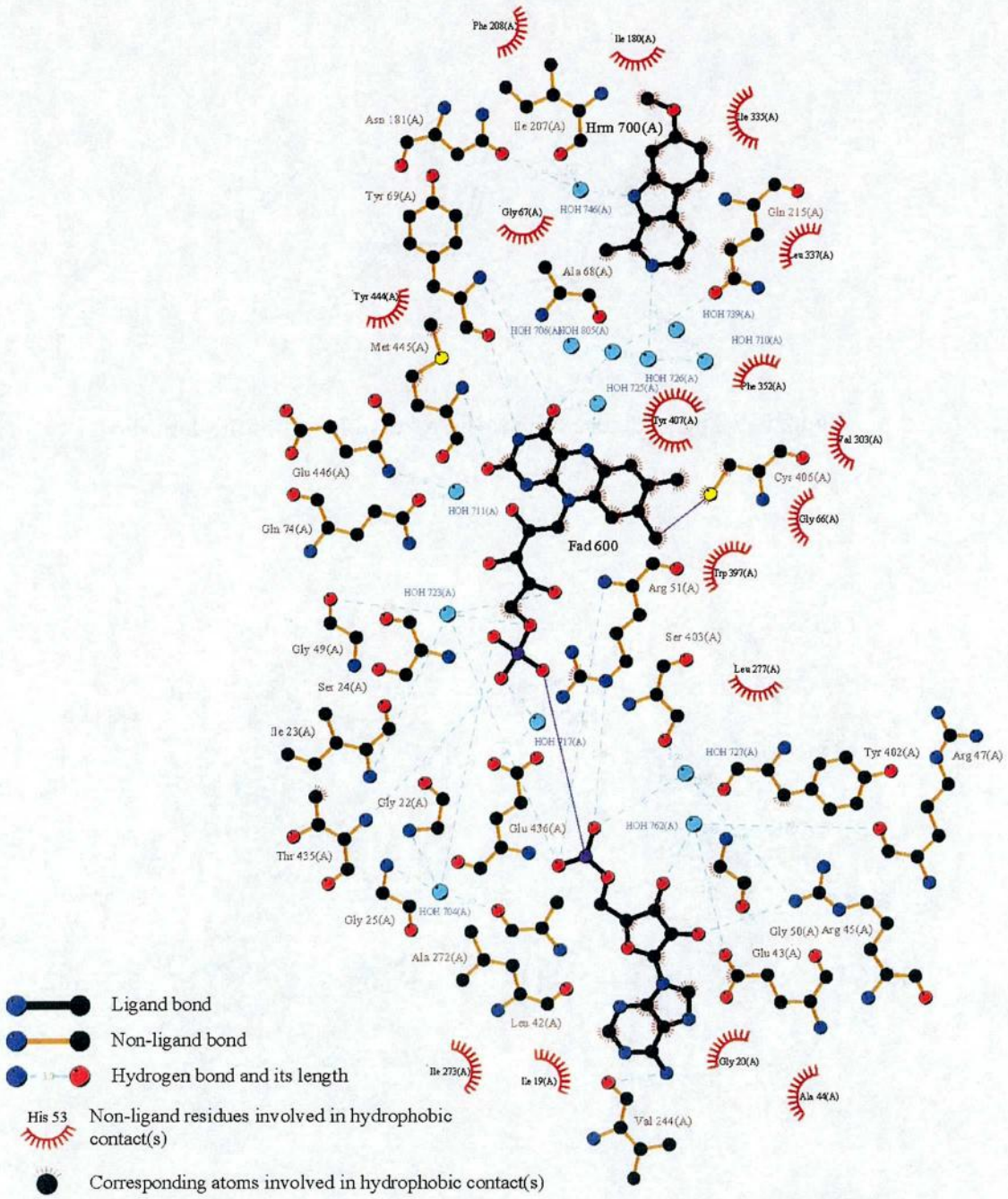

Figure 3-11 The picture of the interactions among FAD, inhibitor(harmine) and human MAOA. This picture was generated by the Ligplot program. (wallace *et al.*, 1995)

3-3. Structural comparisons with other MAOs

3-3-1. human MAOA and human MAOB - structure of the substrate/ inhibitor cavity with specific reversible inhibitor and its specificities

The superposed residues surrounding the substrate/inhibitor cavity of human MAOA, rat MAOA, and human MAOB are shown in Figure 3-12. All 16 residues surrounding the substrate/inhibitor cavity are conserved between human and rat MAOA. In human MAOA, six of the 16 residues differ from the structures of human MAOB.

The structure of human MAOA with harmine is superposed to that of human MAOB with other inhibitors including isatin (pdb code, 1OJA), rasagiline analogue (pdb code, 2C67), and 1,4-diphenyl-2-butene (pdb code, 1OJ9). The positions of the aromatic rings of these reversible inhibitors are highly conserved, as shown in Figure 3-13. Coplanar aromatic rings make π–π interactions with Gln215 of human MAOA or Gln206 of MAOB (Gln215/206). The aromatic rings interact with Phe352/343 and Tyr407/398 at the opposite side of Gln215/206. The molecular structure of the harmine in human MAOA could not be accommodated into human MAOB because of its structural overlap with Tyr326 of MAOB. Thus, Ile335 in MAOA and Tyr326 in MAOB play a crucial role in substrate/inhibitor selectivity. These results are consistent with our previous structural analysis of rat MAOA, and with site-directed mutagenesis studies (Ma *et al.*, 2004b, Geha *et al.*, 2001). The structure of 1,4-diphenyl-2-butene in human MAOB would collide with Phe208 of human MAOA, which corresponds to Ile199 of human MAOB.

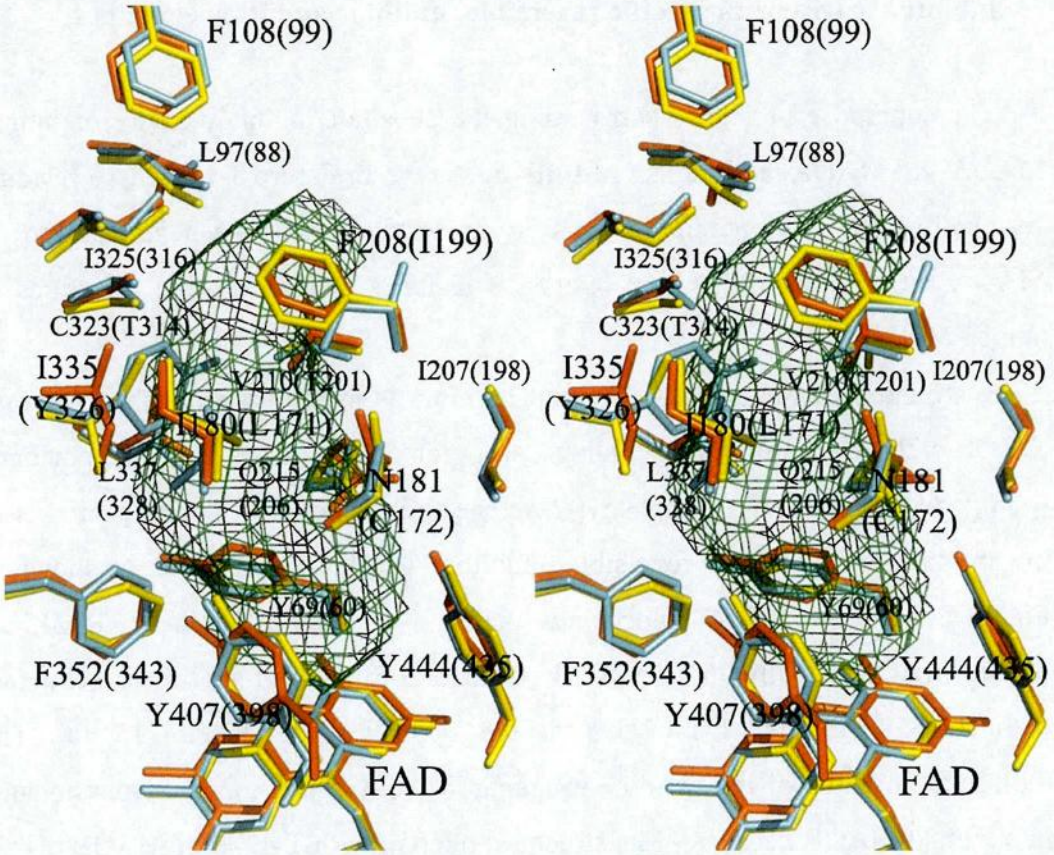

Figure 3-12 Stereoview of the substrate/inhibitor binding sites of human MAOA, MAOB, and rat MAOA. Residues of human MAOA are shown in yellow, rat MAOA in orange, and human MAOB in cyan. The residues that are important in forming the substrate/inhibitor cavity are labeled. The residue numbering is according to the residue positions in human MAOA, which are the same as in rat MAOA. The residue numbers of human MAOB are shown in parentheses. Two residues, I199 of human MAOB and I335 of human or rat MAOA, are present as different rotamers in different complexes. The cavity is calculated by VOIDOO (Kleywegt *et. al.*, 1994) with a 1.57Å radius probe. These models were generated in Pymol (DeLano, 2002) (RMSD was 0.545 Å for human MAOB and 0.612 Å for rat MAOA).

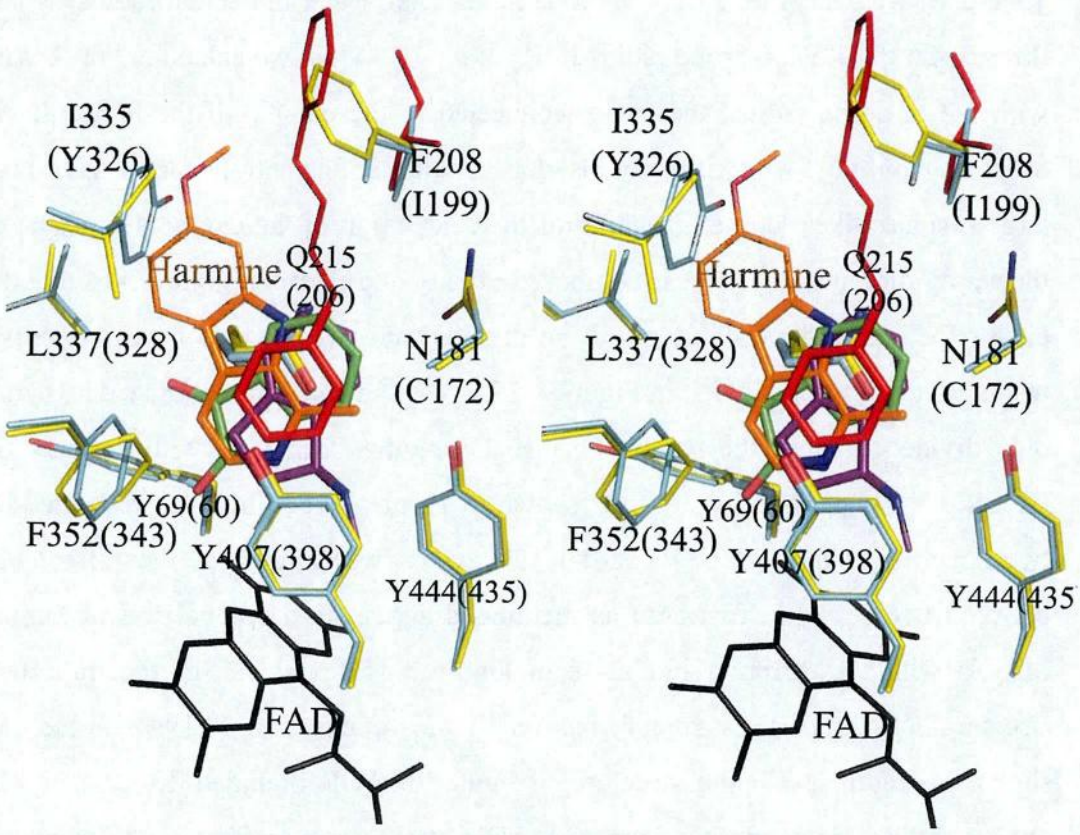

Figure 3-13 Stereoview of structure of the substrate/inhibitor binding sites in human MAOA and MAOB complexed with specific inhibitors. The residues are numbered according to human MAOA, and the numbers in the parentheses are for human MAOB; MAOA and MAOB residues are shown in yellow and light blue, respectively. Inhibitors are colored as follows: orange, harmine; green, isatin (1OJA); purple, rasagiline analogue (2C67); and red, 1,4-diphenyl-2-butene (1OJ9)). FAD is shown in black. Nitrogen and oxygen atoms are shown in blue and red, respectively. I199 of MAOB is present as different rotamers in different complexes. The rotamer of this residue, in MAOB with 1,4-diphenyl-2-butene, is shown in red. The residues Q215 and Y407 that forms important hydrophobic interactions to the inhibitors are shown as thick stick models.

We also compared the shapes and sizes of the substrate/inhibitor cavities between human MAOA and MAOB by using the VOIDOO program. Figures 3-14, 15 and 16 are generated by 1.4 Å probe radius (like water molecular radius) which differ from the 1.57 Å probe radius in Figure 3-12. When we calculated the cavity with 1.4 Å probe radius, the cavity connected to the outside of the molecule. In order to avoid this, we artificially insert a mutation on the entrance loop with more large residues like alanine or valine for the calculation of the cavity. The shape of the cavity for human MAOA is composed of only one cavity in Figure 3-14, but the cavity for human MAOB seems to be divided into two cavities by two specific residues, Tyr326 and Ile199, in Figure 3-15A. We can confirm that the cavity is not only divided because the residues can make another formation with the specific inhibitor, 1,4-diphenyl-2-butene, as shown in Figure 3-15B, but also restricted by two specific residues, Tyr326 and Ile199, which was known as the differences between two subtypes of MAO as mentioned above. In a comparison of human MAOB with the different inhibitors in Figure 3-15A and 3-15B, the important structural characteristic is the formation of the rotamers in Ile199 residue. As shown in Figure 3-13, the structure of human MAOB bounded 1,4-diphenyl-2-butene differs from another human MAOB structure combined with reversible inhibitors in the residue (the rotamer is shown in red). The residue made the restricted form according to kinds of inhibitor.

One little special cavity which has about 51.10 $Å^3$ volume is also generated by changing side chain from Phe208 (MAOA) to Ile199 (MAOB). As to be related to these rotamers, Binda *et al.*(2003) was shown to function as a "gate" in the middle of substrate/inhibitor cavity. We also compared the cavity sizes between human MAOA and MAOB. The two models and the cavities are superposed in Figure 3-16. The cavity size for human MAOA and MAOB are 297.72 $Å^3$ and 366.32 $Å^3$, respectively. The differences of the cavity size between human MAOA and MAOB result in the change of the side chain, Phe208 (MAOA) to Ile199 (MAOB).

The selectivity of the reversible inhibitors is due to the different size and shape of the substrate/inhibitor cavity, restricted by Ile335 and Phe208 in MAOA, which correspond to Tyr326 and Ile199 of MAOB. When the structures of human MAOA with harmine and rat MAOA with clogyline are compared with each other, the side chains of Ile335 have different conformations. The different inhibitors are accommodated by the induced fit of Ile335, as observed for Ile199 of human MAOB (Binda *et al.*, 2003).

From results of these comparisons, we can confirm that these differences of shapes and sizes of the substrate/inhibitor cavity came from characteristic substrates/inhibitors.

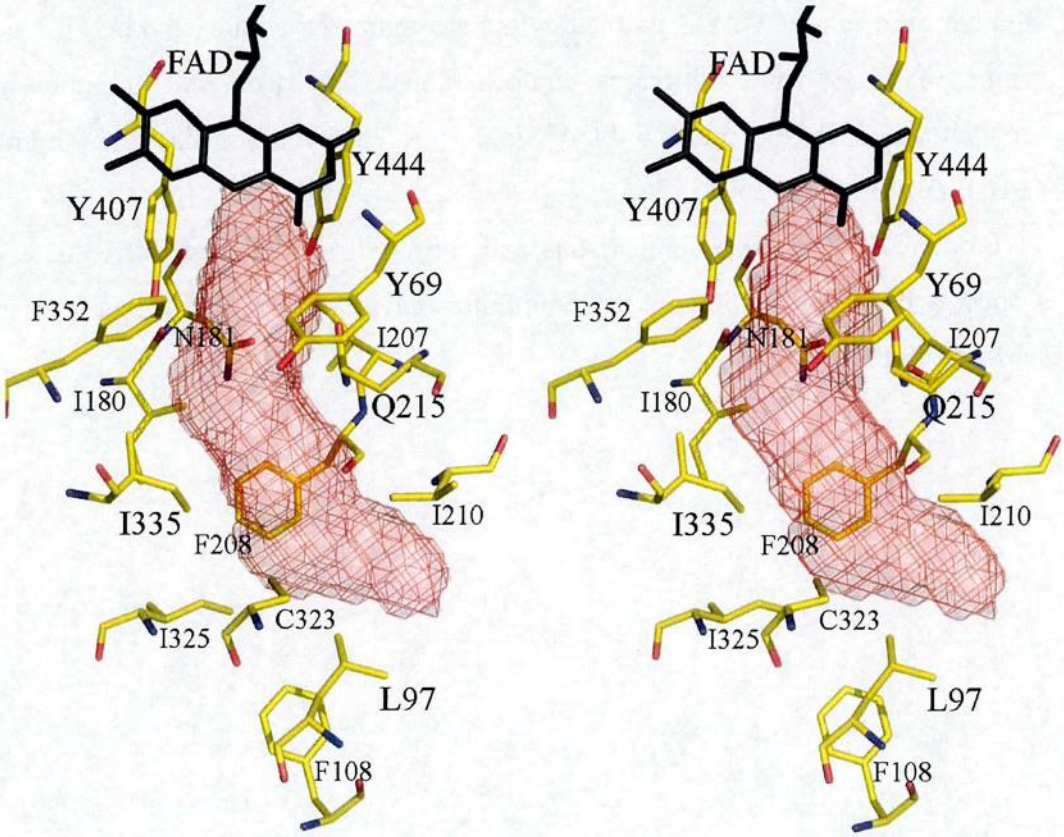

Figure. 3-14 Stereoview of the substrate/inhibitor binding site of human MAOA. The carbon atoms are shown in yellow; nitrogen in blue and oxygen in red. FAD is shown as black without a classification of each of atoms. The residues that are important in forming the substrate/inhibitor cavity are labeled. The cavity shown with a red mesh and semitransparency surface model is calculated by the VOIDOO program (Kleywegt and Jones, 1994) with a 1.4 Å radius probe. The cavity size for human MAOA is 297.72 $Å^3$. This picture was generated by the Pymol program (DeLano, 2002).

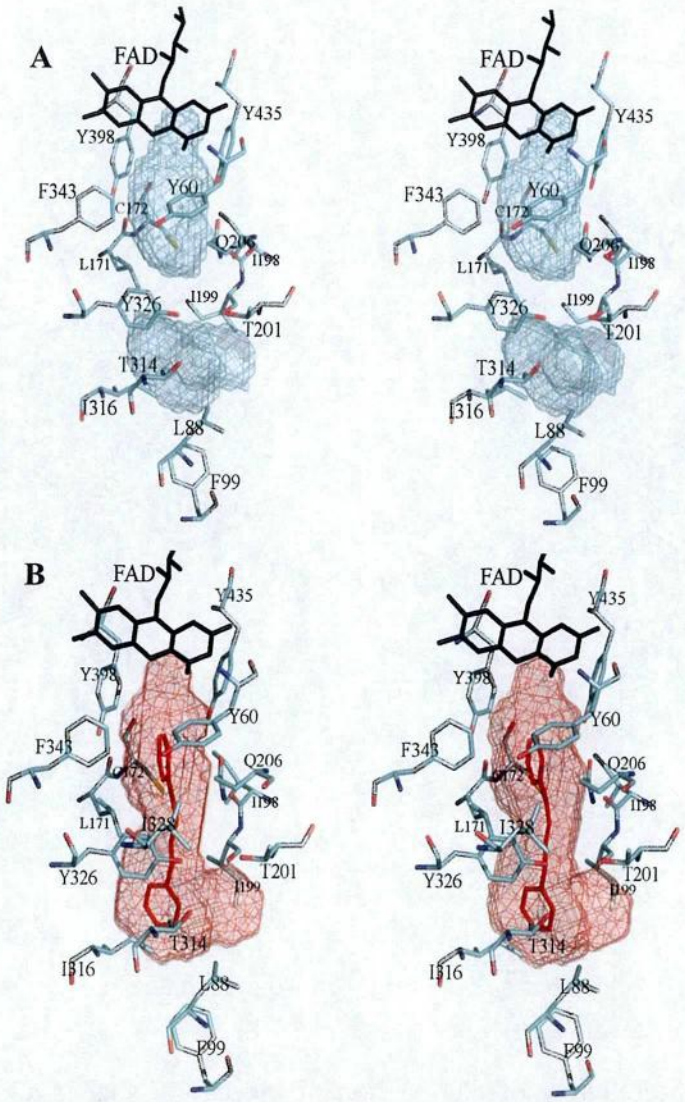

Figure. 3-15 Stereoviews of the substrate/inhibitor binding site of MAOB. The models of human MAOB are binding with the specific inhibitors, rasagyline (A) and 1,4-diphenyl- 2-butene (B). The carbon atom is shown in cyan. ; nitrogen in blue and oxygen in red. FAD and 1,4-diphenyl-2-butene inhibitor are shown in black and red without any classification of each of atoms in the color, respectively. The residues that are important in forming the substrate/inhibitor cavity are labeled. The cavities are shown with a mesh and semi-transparency surface model by cyan and red color with binding rasagyline and 1,4-diphenyl-2-butene, respectively. The cavity sizes for human MAOB complexes with rasagyline and 1,4-diphenyl-2-butene are 366.32 $Å^3$ and 308.66 $Å^3$. All cavities were calculated by the VOIDOO program (Kleywegt and Jones, 1994) with a 1.4 Å radius probe.

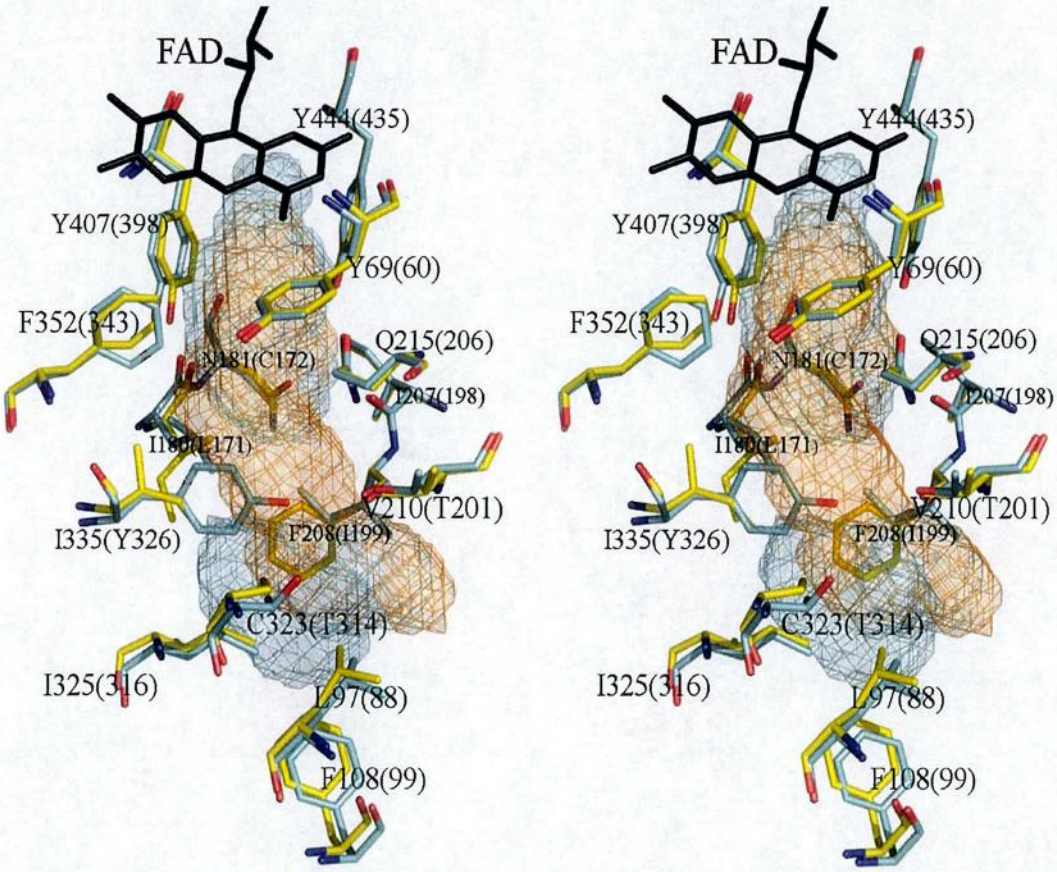

Figure. 3-16 Stereoview of comparison of the cavity shapes and size between human MAOA and MAOB. The carbon atoms are shown in yellow and cyan for human MAOA and MAOB, respectively. The cavities are shown with mesh and semi-transparency surface model by orange and cyan color for human MAOA and MAOB, respectively. The cavity sizes for human MAOA and MAOB are 297.72 $Å^3$ and 366.32 $Å^3$, respectively. These models in this picture were generated by the Pymol program (DeLano, 2002).

3-3-2. Orthorhombic and monoclinic structure of human MAOA

We compared our orthorhombic human MAOA with monoclinic human MAOA by De Colibus *et al.* (2005) (2BXS). The differences of the substrate/ inhibitor cavities between two structures are shown in Figure 3-16 as well as Figure 3-17. In Figure 3-17, harmine and clorgyline are shown in orange and blue color, respectively. There are the significant differences at two loop structures, F208-R217 and F108-P118, as shown in Figure 3-17A. The differences in size and shape of the substrate/inhibitor cavity will be related to the variations of substrate/inhibitor specificities for enzyme of human MAOA. Our human MAOA structure is similar to that of rat MAOA and human MAOB at the loops, but different from those structures of another model by De Colibus *et al.* (2005) (PDB ID: 2BXS), in which it seems that the loop from Ala111 to Val115 is flexible and was not determined. Our structure at high resolution, however, gives clear electron density at this region, as shown in Figure 3-18A.

In 2BXS structure, the loop structure with F208-R217 residues makes a round-folded structure beside the substrate/inhibitor cavity, taking different fold as the present our structure. These differences directly affect the entrance through which the substrate/inhibitor gets into the binding site (red semi-transparent circle in Figure 3-17A). Further more, the location of Q215 is totally different in the different structures. In our structure, the loop, F208-R217, makes one-turned helix and round-folded structure beside substrate/inhibitor cavity. From this structure, aromatic reversible inhibitor can be located in the substrate/inhibitor cavity with the specific interaction between Gln215 and Tyr407.

The loop of A111-V115 with our structure is fully visible in electron density map; it forms the part of entrance for substrate/inhibitor. To confirm that our map is reliable, we used composite-omit-map rather than the 2Fo-Fc map, the later may

introduce more bias from the model structure. Figure 3-18 is shown to the comparison between orthorhombic and monoclinic structures of human MAOA in two loop structures, F108-P118 and F208-R217, with their composite-omit-map. Our loop structures of orthorhombic MAOA are coincided into the composite-omit-map without any disorder in Figure 3-18A, but the structures of monoclinic MAOA with the composite-omit-map had some disorder on the loop as shown in Figure 3-18B. In addition, the DM maps which previously mentioned were also used for a verification of this structure of A111-V115 whether it is clearly located in the wild-type human MAOA or not.

For rational and proper drug design, the three dimensional structures must be based on a self verification such as by using several different maps. In the structural comparison between rat and human MAOA, we could confirm that there was high structural homology in substrate/inhibitor cavity. In contrast to the suggestion by De Colibus *et al.* (2005) that one mammalian form of MAO cannot be unambiguously extrapolated to other mammalian forms because of the differences of the two loop structures F108-P118 and F208-R217 between rat MAOA and monoclinic human MAOA structures, our results indicate that the difficulty of the unambiguous extrapolation must take from not the difference of two loop structures, but the differences in the additional information, because of high structural and sequential identities in the active cavity.

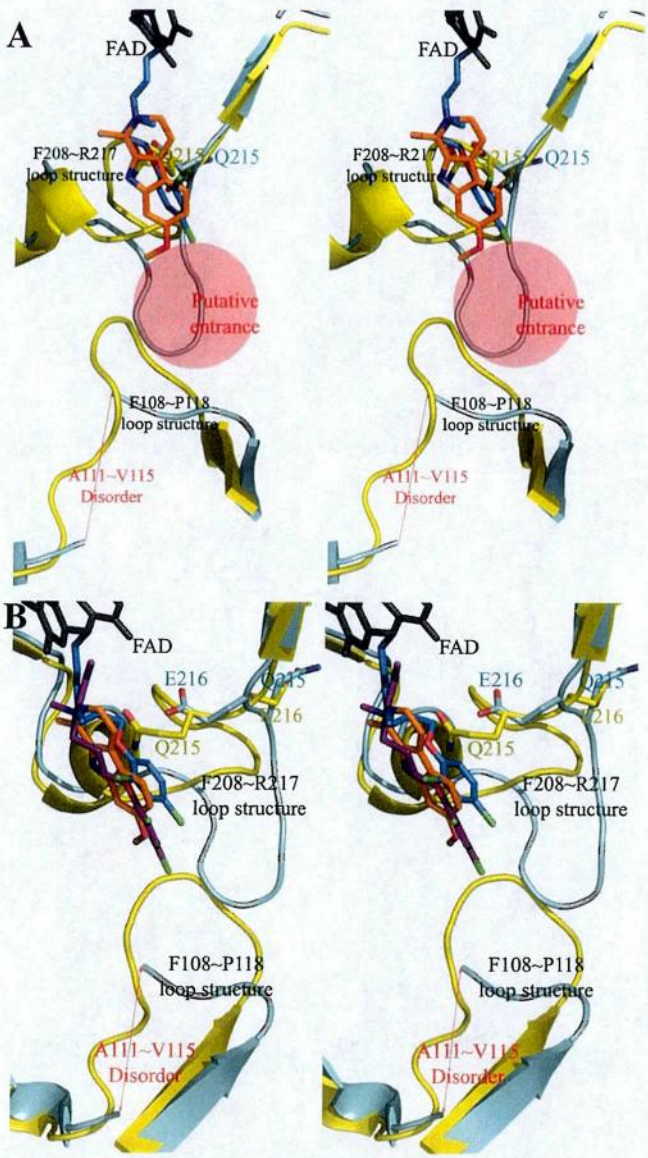

Figure. 3-17 Comparison between orthorhombic and monoclinic structure of human MAOA. Human MAOA is shown in yellow color with the inhibitor, harmine in orange. The monoclinic MAOA (2BXS) is shown in light blue with its inhibitor, clorgyline in blue. (A) Red semitransparent circle represents the putative substrate/inhibitor entrance which calculated from CAVER program. The superposing of the structures is generated by Pymol program (DeLano, 2002). (B) In the case of rat, clorgyline showed in purple here, was bound in a different orientation

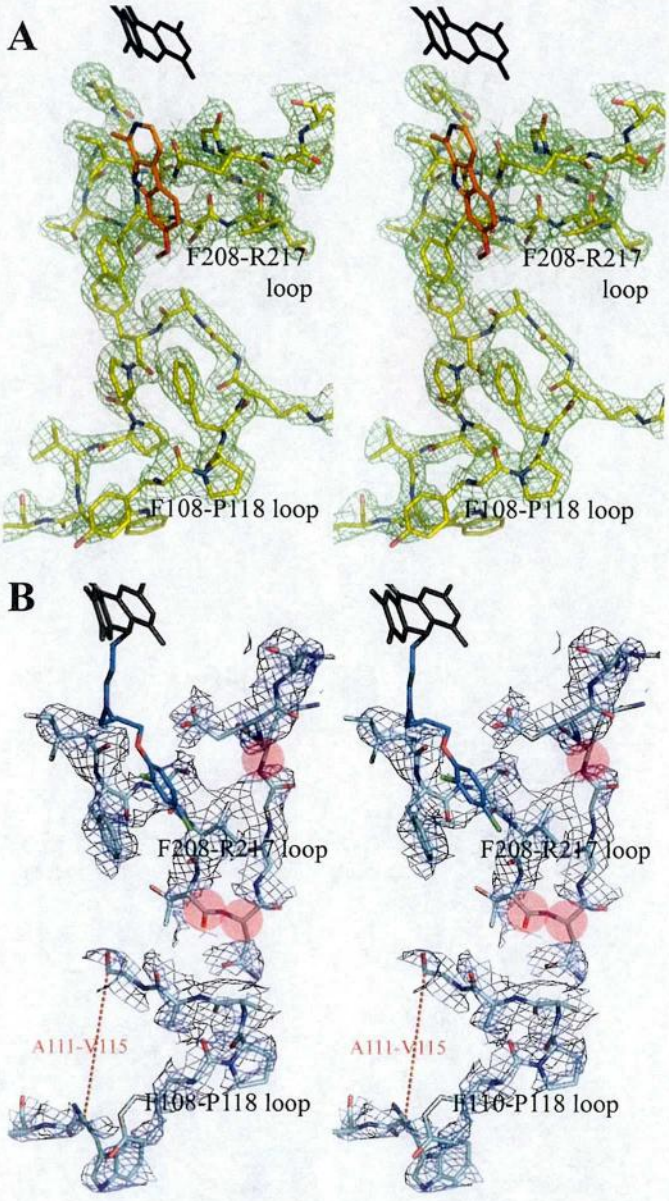

Figure. 3-18 Comparison between orthorhombic and monoclinic structure of human MAOA in two loop structures, F108-P118 and F208-R217. (A) orthorhombic human MAOA is shown in yellow color with the inhibitor, harmine in orange, and with composite-omit-map at 1.0 σ contoured level. (B) The monoclinic MAOA (2BXS) is shown in cyan color with its inhibitor, clorgyline in blue, and with composite-omit-map at 1.0 σ contoured level. A few disordered parts are shown in Red semitransparent circle.

3-3-3. Human and rat MAOA

As mentioned above, unlike rat MAOA and human MAOB which form a tight dimer in the crystals, human MAOA as an orthorhombic crystal was a monomer in the *C222* crystal (Figure 3-19B). In the packing model, this is similar to the model of monoclinic human MAOA. The monoclinic human MAOA published by De Colibus *et al.* (2005) is a monomer in the crystal. The results with the analytic ultracentrifugation showed that monoclinic human MAOA also exists as a monomer in aqueous detergent solutions. Similarly, our orthorhombic human MAOA exists as a monomer, which differed from rat MAOA. This structure indicates that our human MAOA may exist as a monomer in aqueous detergent solutions such as the model of monoclinic human MAOA. Rat MAOA is packing of tetrameric formation as two dimers in the crystal. However, four monomers are packing with two units which are composed of two monomers. Rat MAOA likely forms a dimeric structure in a manner similar to MAOB, *in vivo* (Binda *et al.*, 2002, 2003).

In comparison of human MAOB between two different inhibitors, isatin and 1,4-diphenyl-2-butene, the different rotamer conformations showed that Ile199 exhibits that functions as a "gate" between Tyr326 and Ile199 (Figure 3-13) (Binda *et al.*, 2003). When small inhibitors, like isatin and rasagyline, are bound to the substrate/inhibitor binding cavity, the Ile-199 restricted to separate the cavity as two parts. Here, we will term this form as a "restriction form". However, when a special inhibitor, like 1,4-diphenyl-2-butene, is bound to this cavity, the Ile-199 is rotated to a conformation such one cavity as "open form". In the comparison between rat and human MAOA, the rotamers which are similar to the rotamers in human MAOB are found with Ile335 residue (Figure 3-12).

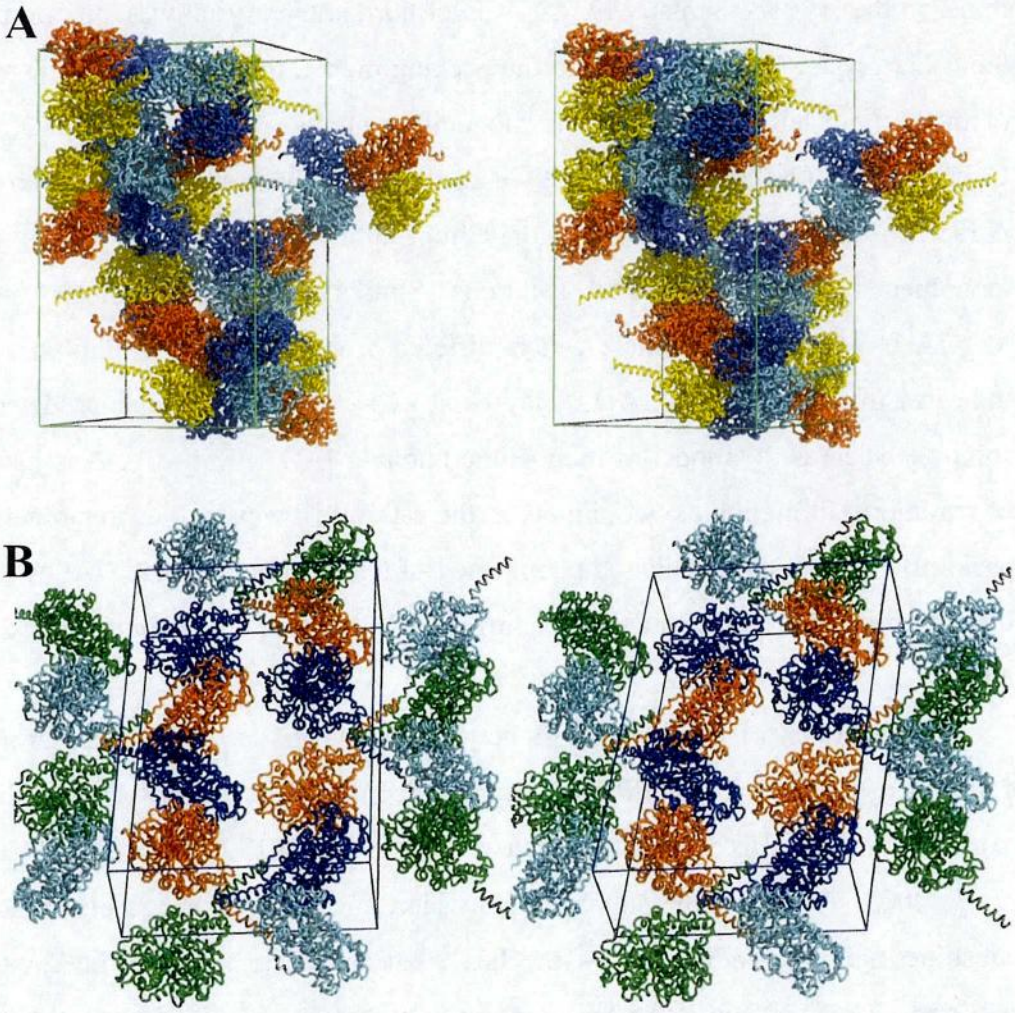

Figure. 3-19 Stereoviews of (A) rat MAOA and (B) human MAOA packing model in $P4_32_12$ and $C222$ crystal, respectively.

3-4. The loop structures at the substrate entrance and its function in enzyme activity

When the structure of the substrate/inhibitor cavity was calculated using the VOIDOO program (Kleywegt and Jones, 1994) with a radius of 1.57 Å, the cavity was completely closed, as shown in Figure 3-20A; when we calculated with a radius of 1.40 Å, however, a narrow path was detected between the cavity and the outside of molecule in Figure 3-20B. The entrance for substrate/inhibitor is surrounded by residues V93-E95, Y109-P112, and F208-N212, which lie in three different loops. The steady-state width of the entrance is too narrow for such compounds as harmine to pass through. We assume that structural fluctuations that enlarge the entrance are essential in order for the cavity to accept substrates. To understand the relationship between the structural fluctuations and the enzymatic reactions, we made a mutation at Gly110 (in the loop 109-112 beside the entrance) in rat MAOA and human MAOA. Although this site is far from the active center, the activity of the purified G110A mutants dropped significantly. Sequence alignments of MAOA (Thr88–Tyr121) and MAOB (Thr79–Tyr112) for a few mammals are conserved well as shown in Figure 3-21. These alignments are also shown to the similarity of mutation point. To further analyze the structure-function relationship at this site, we determined the structure of human G110A. The C_α trace of human G110A was almost identical compared to wild-type MAOA, both in the loop structures and in other parts of the protein, implying that the activity change was derived from a dynamic alteration of the structure of the enzyme (Figure 3-22). To further confirm the role of the flexibility of G110, a G110P mutant was made, which gave this region a highly rigid quality. As expected, the G110P mutant showed an increase of K_m of 19-fold (Table 2). Together with the structural characteristics of the substrate/inhibitor binding site, these results suggest that the loop flexibility is critical for open the entry for substrates/inhibitors.

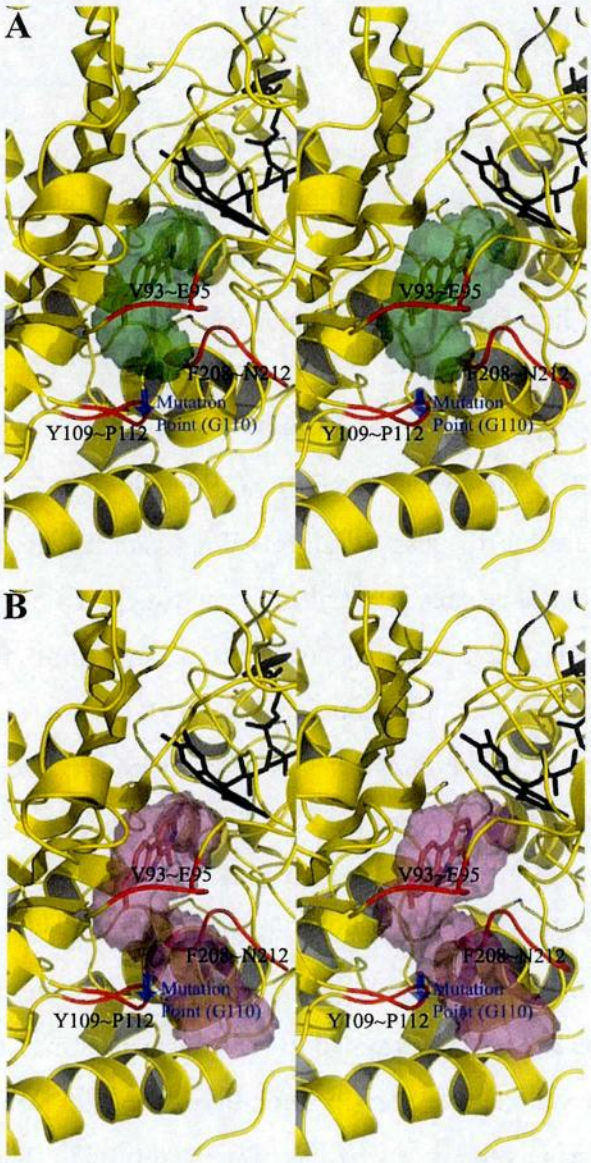

Figure 3-20 Stereoview of (A) the active center cavity which was calculated by VOIDOO (Kleywegt and Jones, 1994) with 1.57 Å probe radius and connected to the surface with ~1.55 Å radius probe, and (B) the pathway from the active center to protein surface. The entrance is surrounded by specific residues: V93-E95 in the K90-L97 loop structure, Y109-P112 involving mutation point, G110, in the F108-P118 loop structure and F208-N212 in the F208-R217 loop structure. This pathway was generated at 1.4 Å probe radius.

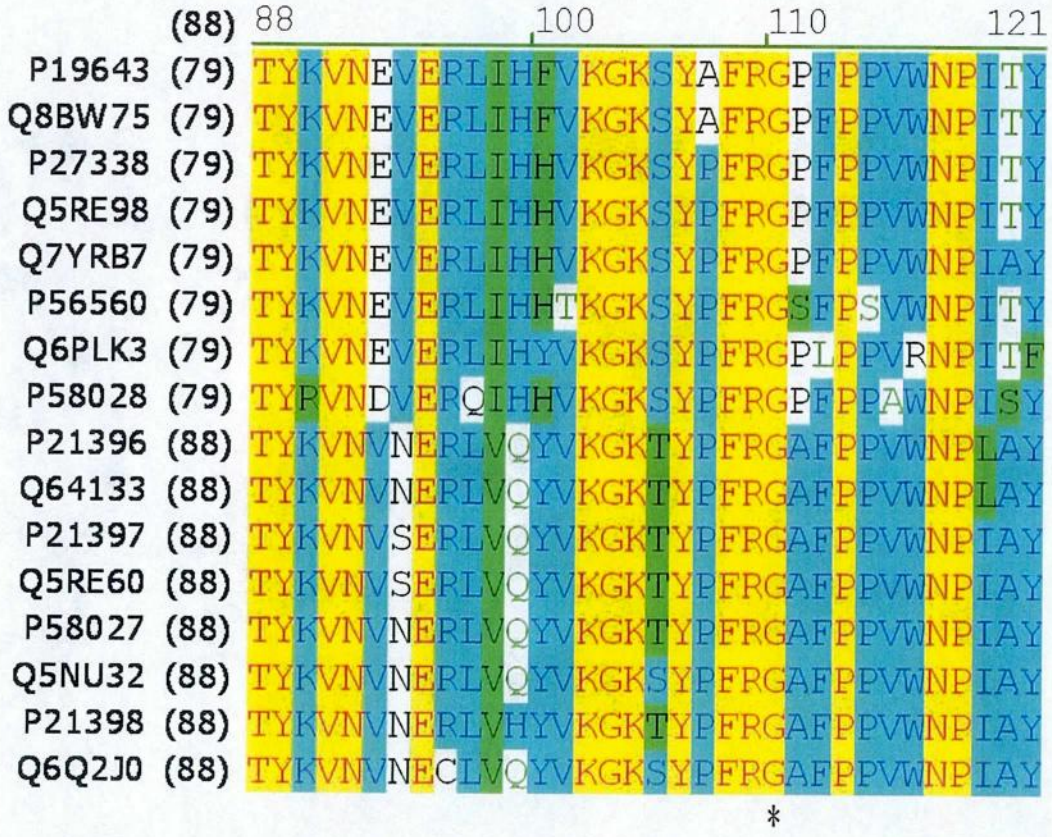

Figure. 3-21 Sequence alignments of MAOA (Thr88-Tyr121) and MAOB (Thr79-Tyr112) for a few mammals. These alignments are shown to the similarity of mutation point. The asterisk means the G110 mutation point.(MAOA/MAOB: rat P21396/P19643, mouse Q64133/Q8BW75, human P21397/P27338, orangutan Q5RE60/Q5RE98, dog P58027/Q7YRB7, bovine Q5NU32/P56560, pig P21398/Q6PLK3, guinea pig Q6Q2J0/P58028)

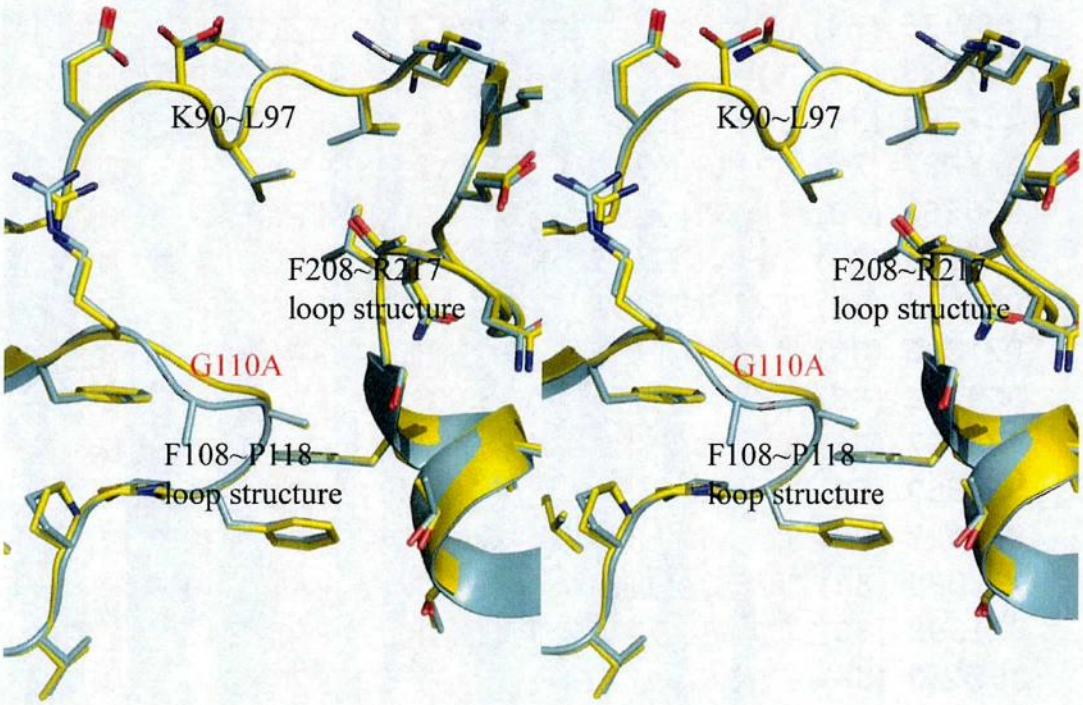

Figure. 3-22 The comparison of the structures between wild type (yellow color) and G110A mutant (sky blue). wild type and G110A at for the putative entrance site are showed in both stick (for side chain) and cartoon (for main chain), the composite-omit-maps were contoured at 2.0 σ level. K90-L97, F108-P118 and F208-R217 loop structures on the entrance (the left) and the active site (the right), respectively.

Table. 2. The kinetic parameters for wild-type and mutant human MAOA.

Enzyme	Solubilized form			Membrane-bound form		
	K_m (mM)	k_{cat} (min^{-1})	k_{cat}/K_m (min^{-1} mM^{-1})	K_m (mM)	k_{cat} (min^{-1})	k_{cat}/K_m (min^{-1} mM^{-1})
Rat WT	0.096±0.016	146±21	1530±143	0.026±0.001	152±5	5792±434
Rat G110A	0.913±0.096	122±10	134±14	0.039±0.003	145±3	3757±268
Rat G110P	1.834±0.178	44±3	24±4	0.184±0.039	142±29	773±14
Human WT	0.117±0.004	181±31	1544±263	0.044±0.004	165±2	3803±349
Human G110A	0.526±0.083	116±13	221±20	0.093±0.003	131±4	1407±41

Interestingly, the mutant enzymes showed more significant changes when they were solubilized from the membrane, as compared to wild-type enzymes. For rat G110A, the K_m for the substrate kynuramine increased nearly 10-fold (0.096 mM to 0.913 mM) compared to the wild-type in the detergent-solubilized form. However, there was very little change in the membrane-bound form (0.026 mM to 0.039 mM). The human mutant also showed similar results. The k_{cat} values for the wild-type and all mutants of rat MAOA or human MAOA are comparable, ranging from 116 to 181 min^{-1} for both the solubilized and membrane-bound forms, except for solubilized rat G110P mutant, which has a k_{cat} of 44 min^{-1}. Since solubilized G110P has a very high K_m value, it is difficult to accurately estimate the maximum activity, because we observed some substrate-inhibition phenomena at very high concentration of substrate (i.e., the activity decreases while the substrate concentration increases too high). Therefore, the low k_{cat} may not reflect a true quality of G110P. These results suggest that the mutation on G110 does not affect enzyme catalytic activity, but rather affects substrate binding, especially in the solubilized form.

These differences in K_m between the membrane-bound and solubilized forms were previously caused by the inactivating effect of the detergent. Although the detergent may have some effects on enzyme activity, it cannot fully explain why the mutants showed significantly bigger change than the wild-type.

Therefore, we conclude that it is the membrane anchoring, but not detergent, that affects enzyme catalytic efficiency (K_m) in MAOA. The decrease of the activity in C-terminal truncated MAOB (Rebrin *et. al.*, 2001) also support the idea that membrane anchoring is essential for MAO's functions.

There is also a possibility that the different K_m values between mutant and wild-type are caused by the larger residues in the mutants, which may block the entrance. If the size plays a major role in blocking the entrance, the mutants should show similar decreases in substrate affinity in both the membrane-anchored and solubilized forms. However, our result showed that only the solubilized form but not the membrane-anchored form had a dramatic change in K_m, indicating that the residue size at G110 is not a major factor that affects the K_m. Instead, flexibility at this site, together with the membrane anchoring, plays the major role. Since the mutation site is far from the active center, and the crystal structure of G110A shows little change in the detailed structure, the only possible change would be in the flexibility of the loop of 109-112, as supported by the above data. From the membrane binding model shown in Figure 3-8, the C-terminal helix and a small part of the enzyme is buried in the membrane, leaving large parts of enzyme in the cytosol. Therefore, it is possible that fluctuations of the extra-membrane domain (e.g., due to Brownian motion) of the MAO enzyme are not synchronized with its transmembrane domain buried in the membrane. This discrepancy between the motions of the extra-membrane and transmembrane domain may therefore cause conformational changes in or around the entrance loops near the active site, which in turn open the entrance for the substrate/inhibitor. Obviously, the flexible G110 is important for inducing this conformational change. Substitution of G110 with

alanine produce a small amount of resistance to this change, but this becomes more obvious when enzyme is solubilized. When G110 is replaced with the rigid residue proline, the resistance to conformational change at the loop becomes more significant, both in membrane-bound and solubilized forms. This model partially explains the role of the C-terminal anchoring of MAOA, and is a novel concept in membrane protein function.

Figure 3-23 shows the models of human monoamine oxidase A as membrane-bound form. These models indicate a closed form (right) and an artificial-opened form (left), based on this concept for membrane protein function, in the entry. The overall model makes a complex with the specific reversible inhibitor, harmine (right).

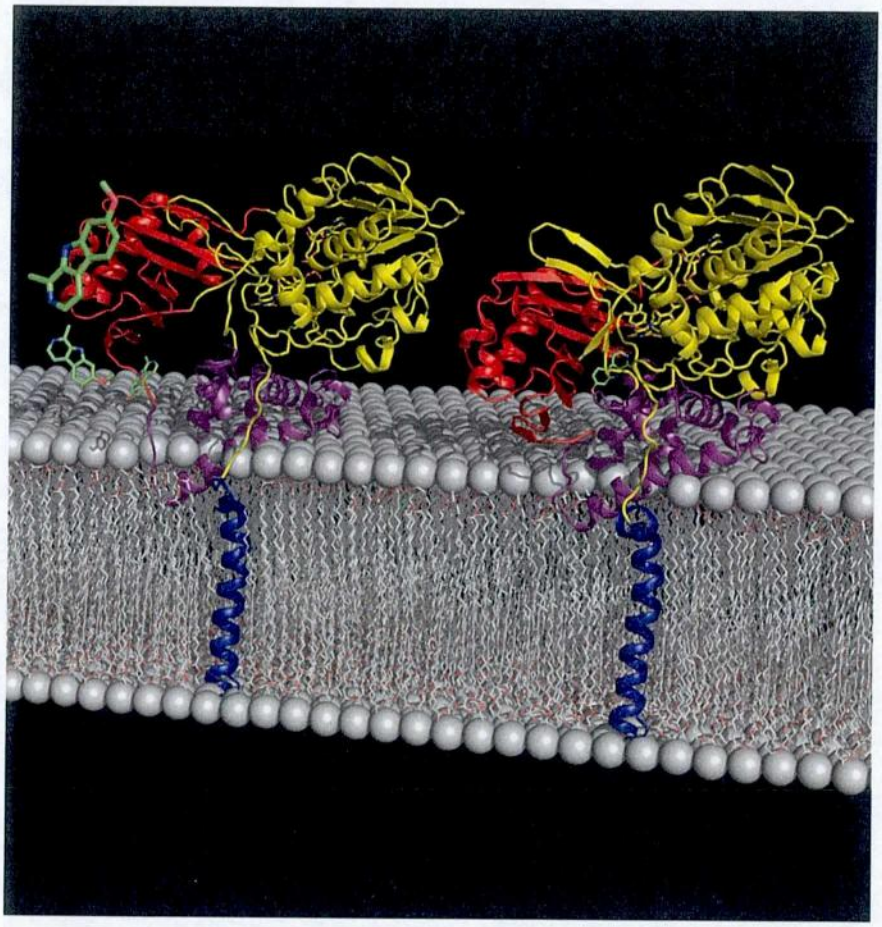

Figure. 3-23 The models of human monoamine oxidase A as membrane-bound form.

Chapter 4. Conclusion

In this research, the structures of human monoamine oxidase A complexed with a reversible inhibitor, harmine, were determined at 2.20Å and 2.17Å resolution for the wild-type and the G110A mutant, respectively. The backbone structure of human MAOA was nearly identical to that of rat MAOA, but contrasted in the important loop structures with monoclinic human MAOA.

We determined three important structural parts for human MAOA in this research. **The first** is the specific residues, Glu215 and Tyr407, for binding between specific reversible substrates/inhibitors and human MAO enzymes, both of MAOA and MAOB. The aromatic reversible inhibitors determined thus far, including harmine, were accommodated in the same substrate/inhibitor cavity by making tight π-π interactions between their aromatic ring and Tyr407. The amide group of Gln215 is interacted with π-π interactions to the reversible inhibitor, either. **The second** structure that was determined is the crucial structure for the specific substrate/inhibitor selectivities in human MAO. The specific selectivity of substrate/inhibitor is due to the structural restriction of Ile335 of MAOA (Tyr326 of MAOB) which makes the different size and shape of the substrate/inhibitor binding cavity. **The final part** is the transmembrane helix structure for which the functional role is unknown. Human MAOA has a transmembrane helix, as did rat MAOA. The helix structure is clearly confirmed in this study. Additionally, **the enzymatic function of C-terminal helix structure** was confirmed through some activity experiments with changing the flexibility of special loop structure on the entrance. The active center cavity was closed in the steady state. Through the results of activity experiment, we knew that movements of the extra-membrane domain fixed to the mitochondrial membrane by the transmembrane helix must change the conformation of the entrance to accept substrates/inhibitors. Together with the structural relationship with the substrate/inhibitor binding site, these

results give a conclusion that the loop flexibility is critical for opening the entry for substrates/inhibitors.

These insights in this research provide important information for a rational and effective drug design. In particular, these will be useful for the drug design of reversible specific inhibitors which affect in symptomatic effects such as to increase the biological duration of monoamine transmitters, as well as in neuroprotective effects such as the prevention or delay of neurodegeneration itself.

References

Arai, R., Karasawa, N., Kurokawa, K., Kanai, H., Horiike, K. and Ito, A. (2002) Differential subcellular location of mitochondria in rat serotonergic neurons depends on the presence and the absence of monoamine oxidase type B, *Neuroscience* **114**(4), 825-835

Bach, A.W.J., Lan, N.C., Johnson, D.L., Abell, C.W., Bembenek, M.E., Kwan, S.W, Seeburg, P.H., and Shih, J.C. (1988) cDNA cloning of human liver monoamine oxidase A and B: molecular basis of differences in enzymatic properties, *Proc. Natl. Acad. Sci. USA* **85**, 4934-4938

Bergfors, T. (2003) Seeds to crystals, *J. Struct. Biol.* **2**, 66-76

Binda, C., Newton-Vinson, P., Hubalek, F., Edmondson, D.E. and Mattevi, A. (2002) Structure of human monoamine oxidase B, a drug target for the treatment of neurological disorders, *Nature Struct. Biol.* **9**, 22-26

Binda, C., Li, M., Hubalek, F., Restelli, N., Edmondson, D.E. and Mattevi, A. (2003) Insights into the mode of inhibition of human mitochondrial monoamine oxidase B from high-resolution crystal structures, *Proc. Natl Acad. Sci. USA* **100**, 9750–9755

Blaschko, H., Richter, D. and Schlossmann, H. (1937) The inactivation of adrenaline, *J. phys.* **90**, 1-17

Brünger, A.T., Adams, P.D., Clore, G.M., DeLano, W.L., Gros, P., Grosse-Kunstleve, R.W., Jiang, J.S., Kuszewski, J., Nilges, M., Pannu, N.S., Read, R.J., Rice, L.M., Simonson, T. and Warren, G.L. (1998) Crystallography & NMR System: A New Software Suite for Macromolecular Structure Determination, *Acta Cryst. D* **54**, 905-921

Callaway, J.C., Brito, G.S. and Neves, E.S. (2005) Phytochemical analyses of Banisteriopsis caapi and Psychotria viridis, *J.Psy. Drugs* **37**, 145

Collaborative Computational Project, No.4 (1994) The CCP4 Suite: Programs for Protein Crystallography. *Acta Crystallogr. D* **50**, 760-763

Cowtan, K. (1994) 'dm': An automated procedure for phase improvement by density modification., *Jnt. CCP4 and ESF-EACBM Newsl. Protein Cryst.* **31**, 34-38

De Colibus, L., Li, M., Binda, C., Lustig, A., Edmondson, D.E. and Mattevi, A. (2005) Three-dimensional structure of human monoamine oxidase A (MAO A): Relation to the structures of rat MAO A and human MAO B, *Proc. Natl Acad. Sci. USA* **102(36)**, 12684-12689

DeLano, W.L. (2002) The PyMOL Molecular Graphics System, *DeLano Scientific*, San Carlos, CA, USA.

Dale, H. H. and Dixon, W. E. (1909) The action of pressor amines produced by putrefaction, *J. Physiol.* **39**, 25-44

Edmondson, D.E., Colibus, L.D., Binda, C., Li, M. and Mattevi, A. (2007) New insights into the structures and functions of human monoamine oxidases A and B, *J. Neural Transm.* **114**, 703-705

Emsley, P. and Cowtan, K. (2004) Coot: model-building tools for molecular graphics, *Ae cta Cryst. D* **60**, 2126-2132

Fowler, J. S., MacGregor, R.R., Wolf, A.P., Arnett, C.D., Dewey, S.L., Schlyer, D., Christman, D., Logan, J., Smith, M. and Sachs, H. (1987) Mapping human brain monoamine oxidase A and B with 11C-labeled suicide inactivators and PET, *Science* **235**, 481–485

Geha, R.M., Rebrin, I., Chen, K. and Shih, J.C. (2001) Substrate and inhibitor specificities of human monoamine oxidase A and B are influenced by a single amino acid, *J. Biol. Chem.* **276**, 9877-9882

Gouet, P., Robert, X. and Courcelle, E. (2003) ESPript/ENDscript: extracting and rendering sequence and 3D information from atomic structures of proteins, *Nucleic Acids Research* **31**(13), 3320-3323

Grimsby, J., Chen, K., Wang, L.J., Lan, N.C., Shih, J.C. (1991) Human monoamine oxidase A and B genes exhibit identical exon-intron organization, *Proc. Natl. Acad. Sci. USA* **88**(9), 3637-3641

Hardegg, W. and Heilbronn, E. (1961) Oxidation of serotonin and tyramine by rat liver mitochondria, *Biochem. Biophys. Acta* **51**, 553-560

Hare, M. L. C. (1928) Tyramine oxidase. 1. A new enzyme system in liver, *Biochem. J.* **22**, 968-979

Ito, A., Kuwahara, T., Inadome, S. and Sagara, Y. (1988) Molecular cloning of a cDNA for rat liver monoamine oxidase B, *Biochem. Biophys. Res. Commun.* **157**, 970-976

Johnston, P. (1968) Some observations upon a new inhibitor of monoamine oxidase in human brain, *Biochem. Pharmacol.* **17**, 1285-1297

Kleywegt, G.J. and Jones, T.A. (1994) Detection, delineation, measurement and display of cavities in macromolecular structures, *Acta Cryst. D* **50**, 178-185

Larkin, M.A., Blackshields, G., Brown, N.P., Chenna, R., McGettigan, P.A., McWilliam, H., Valentin, F., Wallace, I.M., Wilm, A., Lopez, R., Thompson, J.D., Gibson, T.J. and Higgins, D.G. (2007) ClustalW and ClustalX version 2., *Bioinformatics 2007* **23(21)**, 2947-2948

Ma, J. and Ito, A. (2002) Tyrosine residues near the FAD binding site are critical for FAD binding and for the maintenance of the stable and active conformation of rat monoamine oxidase A, *J. Biochem. (Tokyo)* **131**, 107–111

Ma, J., Kubota, F., Yoshimura, M., Yamashita, E., Nakagawa, A., Ito, A., and Tsukihara, T. (2004a) Crystallization and preliminary crystallographic analysis of rat monoamine oxidase A complexed with clorgyline *Acta Cryst. D* **60**, 317-319

Ma, J., Yoshimura, M., Yamashita, E., Nakagawa, A., Ito, A. and Tsukihara, T. (2004b) Structure of Rat Monoamine Oxidase A and Its Specific Recognitions for Substrates and Inhibitors, *J. mol. biol.* **338**, 103-114

Matthews, B. W. (1968) Solvent content of protein crystals, *J. Mol. Biol.* **33(2)**, 491-497

Mitoma, J. and Ito, A. (1992) Mitochondrial Targeting Signal of Rat Liver Monoamine Oxidase B Is Located at Its Carboxy Terminus, *J. Biochem.* **111**, 20-24

Murshudov G. N., Vagin A. A. and Dodson E. J. (1997) Refinement of macromolecular structures by the maximum- likelihood method, *Acta Cryst. D* **53**, 240-255

O'Carroll, A.M., Fowler, C.J., Phillips, J.P., Tobbia, I. and Tipton, K.F. (1983) The deamination of dopamine by human brain monoamine oxidase, *Naunyn-Schmiedeberg's Arch. Pharmacol.* **322**, 198–202

Potterton, E., Briggs, P., Turkenburg, M. and Dodson, E. (2003) A graphical user interface to the CCP4 program suite, *Acta Cryst. D* **59**, 1131-1137

Rebrin, I., Geha, R.M., Chen, K. and Shih, J.C. (2001) Effects of Carboxyl-terminal Truncations on the Activity and Solubility of Human Monoamine Oxidase B, *J. Biol. Chem.* **276**, 29499-29506

Rhodes, G. (2006) Molecular replacement: Related proteins as phasing models, *Crystallography Made Crystal Clear, Academic Press (Elsevier)*, 136-143

Saura, J., Bleuel, Z., Ulrich, J., Mendelowitsch, A., Chen, K., Shih, J.C., Malherbe, P., Da Prada, M. and Richards, J.G. (1996) Molecular neuroanatomy of human monoamine oxidase A and B revealed by quantitative enzyme radioautoradiography and in situ hybridization histochemistry, *Nueroscience* **70(3)**, 755-774

Schnaitman, C., Erwin, V.G. and Greenawait, J.W. (1967) The submitochondrial localization of monoamine oxidase. An enzymatic marker for the outer membrane of rat liver mitochondria. *J. Cell Biol.* **32**, 719-735

Student, A.K. and Edwards, D.J. (1977) Subcellular localisation of type A and type B monoamine oxidase in rat brain, *Biochem. Pharmacol.* **26**, 2337-2342

Stura, E. A. and Wilson, I. A. (1991) Applications of the Streak Seeding Technique in protein crystallization. *J. Cryst. Growth* **110**, 270-282

Vagin, A. and Teplyakov, A. (1997) MOLREP: an Automated Program for Molecular Replacement, *J. Appl. Cryst.* **30**, 1022-1025

Walker, W.H., Kearney, E.B., Seng, R.L. and Singer, T.P. (1971) The covalently-bound flavin of hepatic monoamine oxidase. 2. Identification and properties of cysteinyl riboflavin, *Eur. J. Biochem.* **24**, 328–331

Wallace, A.C., Laskowski, R.A. and Thornton, J.M. (1995) LIGPLOT: A program to generate schematic diagrams of protein-ligand interactions. *Prot. Eng.* **8**, 127-134

Waller, D. A. and Dodson, G. G. (1993) *Molecular structures in biology, oxford science publication*, 1-19

Wang, B.C. (1985) Resolution of Phase Ambiguity in Macromolecular Crystallography, *Methods Enzymol.* **114**, 90-112

Weissbach, H., Smith, T. E., Daly, J. W., Witkop, B., and Udenfriend, S. (1960) A rapid spectrophotometric assay of monoamine oxidase based on the rate of disappearance of kynuramine, *J. Biol. Chem.* **235**, 1160-1163

Westlund, K.N., Krakower, T.J., Kwan,S.W. and Abell,C.W. (1993) Intracellular distribution of monoamine oxidase A in selected regions of rat and monkey brain and spinal cord, *Brain Res.* **612**, 221-230

Weyler, W. and Salach, J.I. (1985) Purification and properties of mitochondrial monoamine oxidase type A from human placenta, *J. Biol. Chem.* **260**, 13199-13207

Youdim, M.B.H., Edmondson, D. and Tipton, F. (2006) the therapeutic potential of monoamine oxidase inhibitors, *Neuroscience* **7**, 295-309

Youdim, M.B.H. and Riederer, P. (1993) The relevance of glial monoamine oxidase-B and polyamines to the action of selegiline in parkinson's disease. *Mov. Disorders* **8**, S8-S13

Zeller, E. A. (1938) On the enzymatic reduction of Histamine and Diamine, *Helv. Chim. Acta* **21**, 880-890

List of publication

Se-Young Son, Jichun Ma, Youhei Kondou, Masato Yoshimura, Eiki Yamashita and Tomitake Tsukihara, (2008) Structure of human monoamine oxidase A at 2.2 Å resolution: the control of opening the entry for substrates/inhibitors, *Proc. Natl Acad. Sci. USA*, 105(15), 5739-5744.